



(ID Modèle = 2081337)

Ineris-207067-2736898-v1.0

21 April 2022

**Resistance of industrial structures to impact from
projectiles of accidental origin**

Ω-23

OMEGA 23

INERIS

controlling risks |
for sustainable development |

FOREWORD

This document has been prepared as part of the support Ineris provides to administrative authorities, by virtue of Article R131-36 of the French Environmental Code.

Ineris shall not be liable, whether directly or indirectly, for any inaccuracies, omissions or errors or any similar occurrences relating to the information used.

The accuracy of this document must be assessed on the basis of the objective knowledge available and, where appropriate, of the current regulations at the date of the approval of this document. Accordingly, Ineris shall not be held liable due to the evolution of these knowledge or regulations after this date. Its mission shall not entail any obligation for Ineris to update this document once approved.

Given the missions entrusted under article R131-36 of the French Environmental Code, Ineris is not a decision-maker. Hence, the opinions, advice, recommendations or equivalent that will be provided by Ineris as part of its missions are solely aimed at assisting the decision-making process. As a result, the responsibility of Ineris cannot replace that of the decision-maker that is therefore, notably, solely responsible for any interpretations made on the basis of this document. Any recipient of the document shall use its results in their entirety or at least in an unbiased manner. The use of this document in the form of extracts or summary notes will be the sole and entire responsibility of the recipient. The same applies for any amendments that may be made thereto. Ineris declines all responsibility for any use of the document outside the purpose of the mission.

Division responsible for the report: Fire, Dispersion and Explosion Department

Authors(s): PRATS FRANCK

Review: LE-ROUX BENJAMIN; HEUDIER LAURE

Approval: PIQUETTE BERNARD – on 21 April 2022

Table of Contents

1	Introduction	7
1.1	Omega Reference systems.....	7
1.2	Scope of application	7
1.3	Regulatory context.....	8
1.4	Structure of the document.....	9
2	Impact phenomena: description and characterisation.....	10
2.1	Past experience.....	10
2.2	General definition	14
2.3	Classification proposed by Eibl: Soft impact / Hard impact	14
2.4	Unified shock characterisation suggested by Koechlin	15
2.5	Summary.....	17
2.6	Behaviour of a structure in the event of a projectile impact	18
2.7	Behaviour of a concrete target against a projectile impact	18
2.8	Behaviour of a steel target against a projectile impact.....	20
3	Methods used to calculate the resistance of structures to the impact of projectiles	21
3.1	Empirical correlations.....	21
3.1.1	Generic formulas (concrete/steel) for local impacts.....	22
3.1.2	Concrete targets and local hard impact	25
3.1.3	Steel target and local hard impact	34
3.1.4	Limits of the empirical models	45
3.2	Analytical methods.....	46
3.2.1	General information.....	46
3.2.2	Models of target global responses	46
3.2.3	Response model translating a localised hard impact.....	48
3.3	Numerical methods.....	51
3.3.1	The “continuous” methods.....	51
3.3.2	The “discrete” methods	52
3.3.3	An alternative: the multi-domain approach.....	52
3.3.4	Main calculation software programs	53
3.3.5	Conclusions	54
4	Protective measures.....	55
4.1	Protective enclosure	55
4.2	Changes to the target’s mechanical properties	55
5	Conclusion	57
6	Bibliographic references	58

FIGURES

Figure 1: Domino effect diagram [IMFRA 2008]	7
Figure 2: Boiler element propelled by rocket effect	10
Figure 3: Accidents involving burst tanks containing pressurised gas - Fragment forming [IMFRA 2008]	10
Figure 4: Properties of typical projectiles likely to be found in industrial environments [MICADO 2002], [SNPE INGENIERIE 1995]	11
Figure 5: Examples of fragment-generating accidents – Consequences of the fragments propelled to nearby entities [BARPI]	13
Figure 6: Mass-spring system associated with the modelling of the impact of a projectile [Koechlin 2007]	14
Figure 7: Shock classification [Koechlin 2007]	16
Figure 8: Soft impact / hard impact field [Koechlin 2007]	17
Figure 9: Example of projectile impact on a concrete target	18
Figure 10: Progression of cracking and formation of the shear cone [May et al. 2005]	19
Figure 11. Different effects resulting from impact on a concrete slab: (a) penetration, (b) cone cracking, (c) spalling, (d) Cracks on (i) the front side and (ii) the rear side, (e) scabbing, (f) perforation, and (g) overall target response [Li 2005].	19
Figure 12: Example of a brittle fracture in a steel target	20
Figure 13: Petalling (left) and punching (right) [IMFRA 2008]	20
Figure 14: Penetration and perforation [IMFRA 2008]	20
Figure 15: Different definitions of critical perforation speed [Li 2008]	22
Figure 16: Coefficient C_i based on the nature of the impacted target [Thor 1961]	23
Figure 17: Scope of application for Thor's equations [Thor 1961]	23
Figure 18: Perforation parameter as per the type of material	24
Figure 19: Thicknesses of perforation based on projectile properties [Micado 2002]	24
Figure 20: Perforation parameter as per the nature of the material	25
Figure 21: Empirical models better suited to industrial issues	26
Figure 22: Shape of the reference projectile	27
Figure 23: Penetration depth based on the impact velocity and mass of the projectile made of “perforating” steel	28
Figure 24: Penetrability coefficient	29
Figure 25: Evolution of K_p depending on the concrete's compressive strength f_c (Li [2005])	29
Figure 26: Shape factor associated with the projectile's impacting part	29
Figure 27: Shape factor associated with the projectile	31
Figure 28: Comparison between different empirical models [Yankelevsky 1997]	33
Figure 29: Comparison of different empirical models [Li 2005]	33
Figure 30: Penetration depth based on the impact velocity and mass of an armor piercing steel fragment	35
Figure 31: Shape of the reference projectile	35
Figure 32: Comparison of the prediction of Corbett et Reid's (1993) empirical models and experimental data with a hemispherical-headed projectile	39
Figure 33: Comparison of the theoretical and experimental results on the series of trials conducted by Lepareux (1989) [Mebarki et al. 2007]	40
Figure 34: Penetration of a cylindrical projectile in a steel target [Mebarki et al. 2007]	40
Figure 35: Normal impact (tilt angle of 0) of a cylindrical projectile on a steel target: plasticised effective volume around the contact area [Mebarki et al. 2007]	41
Figure 36: Comparison between the Lepareux (1989) experimental depths of penetration and the Ineris model	42
Figure 37: Comparison between the Borvik (2003) experimental depths of penetration and the theoretical Ineris model	42
Figure 38: Maximum speed of penetration of a 15 mm-thick mild steel plate (Case no. 1)	44
Figure 39: Critical kinetic energy of perforation of a 15 mm-thick hardened steel plate (Case no. 1)	44
Figure 40: Modelling of a soft impact: determining the impact force [Riera 1968]	47
Figure 41: Process of penetration of the projectile in the target on impact [Corbett and Reid 1996]	50
Figure 42: Two-step penetration model [Yankelevsky 1997]	50
Figure 43: Illustration of the impact of a projectile on a concrete slab [Teng 2004]	51
Figure 44: Simulation of the impact of a deformable projectile on a concrete slab using the Discrete Element Method ([Sawamoto et al. 1998] on the left, [Koechlin 2007] on the right)	52

Figure 45: Combined method of finite elements and discrete elements suggested by Cundall (2003) [Frangin 2008].....52

Figure 46: Simulation of the impact of a projectile on a reinforced concrete slab [Frangin 2008].....53

Figure 47: Coupled approaches – Impact of a deformable body on a rigid structure [Riera 1968].....53

Figure 48: Example of a metal protective wall and a reinforced concrete protective enclosure for a public-access building55

Figure 49: Example of a splinter-proof grating, a) Ineris cage made from splinter-proof grating (4 m x 4 m x4 m) for burst tests, b) deformation of the grating caused by a projectile, c) attachment to a metal frame55

Figure 50: Brickwork and metal reinforcement.....56

Executive summary

This **Ω-23** report is a summary of the current scientific knowledge identified by Ineris in order to determine the effects of projectile impact on the concrete or metal structures found on industrial sites (fire tanks that may disrupt response capabilities if destroyed, hazardous material storage (pressurized vessels, atmospheric tanks, pipework systems, ...) or control rooms, the destruction of which may also aggravate the situation). In the event of an industrial accident, an equipment explosion may produce fragments that, when propelled, may impact or even perforate nearby equipment and, as result, trigger a series of disastrous consequences called domino effect. Accidentology shows that this phenomenon may be the source of catastrophic accidents and lead to numerous casualties. The purpose of this Omega reference report is to describe the phenomena and modelling tools that can be used to predict the structures behavior when damaged by a projectile:

- Empirical correlations that are most frequently used. Experimental databases are used to establish relationships between penetration depth/perforation limit thickness and the main parameters of modelling (impact velocity, geometry/projectile dimensions, projectile characteristics, ...). This approach is suitable to evaluate the local effects generated by non-deformable projectiles impact on materials such as concrete, reinforced concrete or steel.
- Analytical methods generally based on resolution of the differential equations describing the system. It makes possible the evaluation of the local response as well as the overall response on simple structure. This approach allows to not oversize the means of protection to implement compare to an empirical approach.
- Numerical approaches based on finite element methods or discrete methods to combine the projectile and target responses and determinate more realistic simulations. This approach completes the above approaches for composite materials (i.e reinforced concrete) or complex structures.

Use the link provided below for quotations:

French national institute for industrial environment and risks (Ineris), Resistance of industrial structures to impact from projectiles of accidental origin - Ω-23, Verneuil-en-Halatte : Ineris - 207067 - v1.0, 21 April 2022.

Keywords:

safety studies, industrial accident, projectile impact, resistance of concrete or metal structures, states of the art, modelling tools: empirical correlations, analytical methods, numerical approaches

1 Introduction

1.1 Omega Reference systems

OMEGA (Ω) reference systems are a comprehensive repository that formalise Ineris' expertise in the field of accidental risks. This repository covers the following topics:

- risk analysis;
- the physical phenomena involved in accidental situations (fires, explosions, BLEVEs, etc.);
- the control of accident hazards;
- the methodological aspects for conducting regulatory work (hazard studies, critical analysis, etc.).

The purpose of these reports is to present the knowledge which is considered as consolidated at the time of drafting. These reports are made available to those involved in controlling accident hazards, who will make good use of them within the scope of their responsibility. Some of these reports are translated into English to encourage their distribution. The concepts presented in these reports are not intended as substitutes for regulatory provisions.

1.2 Scope of application

This Ω -23 report is a summary of the current scientific knowledge identified by Ineris in order to determine the effects of projectile impact on the concrete or metal structures found on industrial sites (pressure vessels, metal tanks, pipework systems, fire tanks) that may disrupt response capabilities if destroyed, hazardous material storage or control rooms, the destruction of which may also aggravate the situation).

In the event of an industrial accident, an equipment explosion may produce fragments that, when propelled, may impact or even perforate nearby equipment and, as result, trigger a series of disastrous consequences called the domino effect. Accidentology shows that this phenomenon may be the source of catastrophic accidents and lead to numerous casualties.

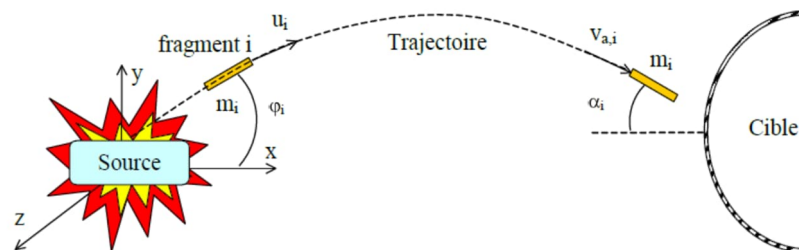


Figure 1: Domino effect diagram [IMFRA 2008]

The risk of equipment being severely damaged following impact by a projectile depends on numerous factors, such as:

- the fragment's mass and speed;
- the fragment's shape and materials (the projectile's deformability upon impact with the target);
- the contact surface on the target;
- the target's thickness, its mechanical properties and the level of pretension of the tank wall or the pipework due to the product's storage conditions;
- the angle that the target and projectile form upon impact.

The purpose of this Omega reference system is to describe the phenomena and modelling tools that can be used to predict the structures' behaviour when damaged by a projectile.

In particular It can be used to answer the following questions:

- What are the fracture mechanisms involved when a projectile impacts a structure?
- Can the projectile penetrate the wall of a structure, facility or equipment and penetrate and perforate it? Will the structure be damaged, or will it remain intact?

- The consequences for a structure – a pressurised vessel for example – after it has been struck by a projectile, and especially in terms of domino effects, are high-stakes issues. Once the structure is impacted, is it weakened enough to generate a secondary accident?

This is the first version of this reference system.

1.3 Regulatory context

The topic of the effects of propulsion is mainly addressed in French law through:

- Regulations for the pyrotechnics sector: inter-ministerial circular of 20 April 2007 [2007-04] *“pertaining to the enforcement of the Order of 20 April 2007 setting the rules pertaining to risk assessment and prevention of accidents in pyrotechnic facilities”*;
- Technological Risk Prevention Plans: circular of 10 May 2010 [2010-12] *“summarising the methodological rules applicable to hazard studies, the assessment of the at-source risk reduction approach, and the technological risk prevention plans (TRPP) in facilities classified under the Law of 30 July 2003.”*

We have decided to include below the extracts of these circulars that specifically address the effects of projectiles.

It must be emphasised that this issue is more specifically addressed through:

- the determination of the areas of effects. In this respect, the “Pyrotechnics” regulation describes the method used to calculate projectile distances based on the mass of the explosive materials.
- the consideration of the *“domino effects generated by fragments on nearby facilities and equipment”*. Based on past experience, over one third occur following impact by “fragments”.

To this end, regulations require that applicable past experience be mentioned in the hazard studies. However, there is no specific mention – except in the “pyrotechnics field” – of a method unanimously recognised by industrial professions that assesses the effects of projectiles on industrial equipment.

This report aims to provide possible answers by presenting a summary of the current scientific knowledge.

Extract from the circular of 10 May 2010:

“Regulatory texts have always addressed in the most specific manner these effects [Editor’s Note: effects of a projectile on a classified facility]. A recent accident (explosion of road tankers carrying LPG with long-distance propulsion of tank components) is an opportunity to look back at the procedures for taking these effects into account for the control of technological risks.

When violent events lead to the rupture of a tank (explosion of a gas tank, a silo, etc.) or the fragmentation of stored products (e.g. explosion of an ammunition depot), fragments may be propelled (generally through the blast effect).

However, the scientific community knows extremely little about these effects. For this reason, only the domino effects triggered by fragments on nearby facilities and equipment are intended to be taken into account in hazard studies (such an instruction is also valid for facilities subjected to a single authorisation). For longer-distance projectile effects, current scientific knowledge does not provide sufficiently accurate and credible predictions of the description of the phenomena in order to determine the public course of action.

You may therefore ask operators, when submitting hazard studies to you, to only cite known past experience relating to projectiles in similar accidents to the ones described in the hazard study. However, if this information on accidents that affected similar facilities must be collected in order to ensure operator transparency in the hazard study and State transparency in its analysis, the collected information should not be taken into account in the procedures provided for in Paragraphs 2 and 3 of this first section of circular.

However, I ask you to make an exception to this rule for the pyrotechnics field that – for historical reasons – has sufficiently reliable data on the fragments generated by certain civil or military pyrotechnical products¹³.

For this type of product there are calculation formulas that define the propulsion effect areas¹⁴, which can in certain cases exceed the areas generated by other types of effects. Procedures for taking into account these effects in the instruction of the hazard studies are more precisely laid out in sub-paragraph “1.2.7 Pyrotechnics Field” below.

¹⁴ Formulas of the inter-ministerial circular of 20 April 2007.

Extract from the inter-ministerial circular of 20 April 2007:

“The areas of effect in pyrotechnics have been historically calculated using calculation formulas established through trials (real or model-based). These areas of effect, which in reality correspond to the areas delimited by the effect thresholds listed in Article 11 of the Order of 20 April 2007, are supported by solid past experience.

As a result, the areas determined using the calculation formulas listed below [...], which are contained in the Order of 26 September 1980 that sets the rules for determining isolation distances for pyrotechnic equipment, correspond to the areas required in the Order of 20 April 2007 and should not be called into question.

The following table determines the size of the areas of effect on bare land (and depending on Q, the net mass of explosive materials excluding their casing) for objects that would propel multiple fragments. These values can be used as a default in other configurations, but other case-by-case basis approaches can also be used. The areas of effect are determined from the edges of the load.

a) If $Q > 100$ kg

Area designation	Z1	Z2	Z3	Z4	Z5
Distance R (m) from the edges of the load Q (kg)	1) Net mass of explosive materials excluding their casing is less than 750 g				
	$0 < R1 \leq 15$	$< R2 \leq 90$	$< R3 \leq 200$	$< R4 \leq 60 Q^{1/6}$ or 300 if $300 \geq 60 Q^{1/6}$	$< R5 \leq 120 Q^{1/6}$ or 600 if $600 \geq 120 Q^{1/6}$
	2) Net mass of explosive materials excluding their casing is over 750 g				
	$0 < R1 \leq 25$	$< R2 \leq 135$	$< R3 \leq 300$	$< R4 \leq 75 Q^{1/6}$ or 400 if $400 \geq 75 Q^{1/6}$	$< R5 \leq 150 Q^{1/6}$ or 800 if $800 \geq 150 Q^{1/6}$

b) If $10 \text{ kg} \leq Q < 100 \text{ kg}$: the distances listed in the previous table can be reduced by one third;

c) If $Q < 10 \text{ kg}$: the limits of the areas of effect are to be defined through a specific study.

If materials or objects present both a mass explosion hazard and a high risk of projectiles (more than 150 g over a distance of at least 15 m), the areas of effect to adopt are the widest extent of those of the product or its casing, which have been determined for these materials or objects considered as belonging, on the one hand, to Division 1.1., and on the other hand, to Division 1.2.”

1.4 Structure of the document

The document presents the following, in order:

- the physical phenomenon of an impact (Chapter 2);
- the empirical, analytical and/or numerical models generally used to predict the behaviour of a structure subjected to an impact (Chapter 3);
- the possible means of protection in the event of a proven failure (Chapter 4).

2 Impact phenomena: description and characterisation

2.1 Past experience

The projectiles involved in industrial accidents can be very different. Precisely defining what the projectiles will be (shape, dimensions, nature) and their ballistic characteristics (speed, angle of departure...) is complicated. This is mainly due to the diversity of equipment and buildings as well as the complexity of their fracture mechanics.

For example, a metallic enclosure can burst and propel fragments towards its surroundings. If it contains pressurised gas, their number generally varies from 1 to 4 and their distance does not exceed 200 m. The main types of fragments are the entire tank, the tank's shell, the dome of the tank attached to the shell, and the dome of the tank on its own. In the case of liquefied gas, the projectile (chiefly the tank bottom and flattened sheet fragments) may also be subject to a rocket effect, which means it is propelled during its flight by the fluid phase change (Figure 2).



Figure 2: Boiler element propelled by rocket effect

Date	Location	Material	Type of tank	Burst tank effects	Cause
2006	Georgia	O ₂	Gas cylinder (gas station)	Fragments projection from 100 to 150 m	-
2000	United States	Acetylene / O ₂	Cylinder	Fragment discovered t 1.8 km from the source	-
1999	France (Saint-Denis)	LNG	Car tank	Tank projection at 50 m	Filling pressure error (200 b instead of 20 b)-Design pressure: 80 b
1998	France (Saint-Martin d'Herès)	O ₂	Gas cylinder (5 liters)	Fragments projection up to 200 m	Fire
1998	France (Saint-Martin du Var)	H ₂	O ₂ gasometer	Projection of the dome (1060 kg) at 135 m	Accidental entry of H ₂ in O ₂ gasometer
				Projection of the shell (1150 kg) at 33 m	
1988	France (Saint-Fons)	H ₂	3000 l tank (diam. = 570 mm- length = 14 m)	Projection of fragments: -183 kg at 22 m, -33 kg at 145 m.	Hydrogen embrittlement of steel
1975	United States	Cl ₂	Rail tank	Projection of a part of the tank at 150 m	-

Figure 3: Accidents involving burst tanks containing pressurised gas - Fragment forming [IMFRA 2008]

The projectile can also be composed of building structure components (bricks, rubble, trusses...) put into motion by an internal explosion.

Speed upon impact ranges from a few meters per second to speeds exceeding a hundred meters per second in the most extreme cases (rocket effect).

A more wide-ranging examination of projectiles recovered after accidents on industrial sites [MICADO 2002] leads us to consider four major types of projectiles (generally associated with accidents in storage areas) to which are associated typical impact speeds;

- **a 35 kg valve (bulky projectile):** This is a component with a low (cross-section / mass) ratio. With a small explosion blast surface, its speed of propulsion will be rather low. To give an idea of the scale, for a 300 mbar explosion lasting 300 ms, the propulsion speed is approximately 15 m/s.
- **a 6-inch tube (slender projectile)** (mass of approximately 25 kg for a length of 1 meter): This type of component has a higher (cross-section / mass) ratio than a valve. Its initial speed is therefore higher than that of a valve for an identical initial event. As a result, a speed twice as high as that of the valve is retained.
- **a tank dome** (mass of approximately 1 ton): This type of component is generated when a tank explodes (with or without an internal explosion). A certain number of studies, in particular those conducted by Holden, forecast a high maximum speed (in the range of several hundreds of m/s) as the initial speed. However, for such parts, aerodynamic braking is very quick, particularly at high speeds, which means that impact velocities are significantly lower than the initial velocities.
- **0.1 and 1 kg parts:** These are parts from rotating machines in which the rotating speed of the rotating parts can reach several thousand rotations per minute.

Typical projectile	Apparent surface (m ²)	Typical impact velocity (m/s) ⁽¹⁾		
		V ₁	V ₂	V ₃
35 kg valve	0.06	15	50	150
6-inch tube (mass approx. 25 kg for a length of 1 m)	0.09	30	100	200
Tank dome (mass approx. 1 ton)	0.5	50	150	250
0.1 and 1 kg parts	0.01	100	300	-

⁽¹⁾ For each of these projectiles, 3 typical impact velocities are retained: low velocity, high velocity and median velocity. These typical velocities in the subsonic field are those retained in the [SNPE INGENIERIE 1995] study and can be used to assess the vulnerability of industrial equipment subjected to impact from projectiles and likely to trigger domino effects.

Figure 4: Properties of typical projectiles likely to be found in industrial environments [MICADO 2002], [SNPE INGENIERIE 1995]

Furthermore, an analysis of past accidents (Figure 5) shows that there may be diverse consequences to the propulsion of this type of fragment: injury or loss of life, damage to building structures (collapse), or loss of integrity of industrial equipment (ruptured tanks or pipework), which can in turn generate other accidents by a domino effect.

Year	Location	Triggering event	Fragments formed	Consequences for the surrounding area
1947	Brest	Maritime and coastal transport: Explosion on a ship carrying nitrate	Numerous projectiles formed	"The city was bombarded and sustained substantial damage (gas factory and oil depots on fire...)"
1969	Hungary - Repcelak	Basic chemical industry: BLEVE of a vertical liquid CO2 tank => BLEVE of a second tank by domino effect	<ul style="list-style-type: none"> - propulsion of a third tank by domino effect - Large fragments from the 2 BLEVEs were propelled to a distance of up to 400 m; - Two weighing 2.8 tons were found 150 m and 250 m away 	<ul style="list-style-type: none"> - A tank was blasted into a laboratory located 30 m away - The projectiles from the 2 BLEVEs killed 4 people
1969	Douai	Drinks industry: Explosion of an NH3 tank in a room	Bottom of the tank propelled to a distance of 15 m	Opening of a 2 m ² hole in a (25 cm) wall
1970	United-States - Crescent	Rail transport: Derailment of 9 propane carriages, BLEVE of several carriages	<ul style="list-style-type: none"> - A carriage fragment hit the roof of a service station - Other fragments were propelled to a distance of 180 m (1st BLEVE) and 500 m (2nd BLEVE) 	<ul style="list-style-type: none"> - Collapse of the service station - The propelled fragments (BLEVE from the other carriages) led to the explosion of the last two carriages
1981	Villeurbanne	Wholesaling of non-agricultural intermediate products: Fire and explosions	<ul style="list-style-type: none"> - Metal beams propelled to distances ranging from 5 to 200 m - propulsion of other missiles (5 kg metal boxes, spray cans) 	The propulsion of the beams killed one person and seriously injured 5 others
1982	Venezuela - Tocoa	Electricity production and distribution: Explosion of a 40,000 m ³ tank filled at 40% of FO	Propulsion of the frangible roof into the 33,000 m ³ basin	Rupture of an FO line => Basin fire
1988	Norway - Porsgrunn/Bamble	Basic chemical industry: Explosion of an MVC cloud	Propulsion of missiles to a major ethylene pipe	Pipe did not burst: "worsening [by domino effect] was narrowly avoided"
1989	Lithuania - Jonova	Basic chemical industry: Fertiliser plant: rupture of an NH3 tank	Propulsion of the tank against the retaining wall	Damage to the retaining wall

1991	Berre l'Etang	Basic chemical industry: Rupture of a 6" ethylene pipe caught in a torch fire	Propulsion of a section close to another pipe where the torch fire occurred	Explosion of the second pipe
1992	Verdun	Public prerogative service: Explosion of the overlying gas in two 100 m ³ FOD tanks	Propulsion of the 1st vessel. Propulsion of the 2 nd tank (rocket effect) 50 m high. It then landed outside the site	The 1st tank landed on the boiler room
1993	La Voulte	Rail transport: Derailing of 20 carriages filled with petrol. Explosion of 3 cisterns - Petrol infiltration in the sewers	Propulsion of manhole covers to several meters away	Destruction of a building containing a lifting station
1994	United-States – Belpre	Basic chemical industry: Explosion of a polymerisation reactor (rubber manufacturing)	Flying debris in the direction of a storage and tank park	Pierced tanks => Fire => Fire spread to styrene and FOD vessels
1994	United-States – Sergeant Bluff	Basic chemical industry: Explosion in an ammonium nitrate production unit	Propulsion of a missile to a 3,800 m ³ ammonia storage facility	Storage vessel pierced due to the formation of a 15 cm hole => 30 kg/s leak, formation of an NH ₃ cloud
1998	Mauguio	Other retail goods in specialised stores: Explosion of five 13 kg gas cylinders	Fragments propelled dozens of meters away Propulsion of a piece of a storage cabinet towards a building located 200 m away	The piece of the storage cabinet embedded into the building's cladding
1999	Turkey - Dortyol	Wholesaling of non-agricultural intermediate products: Rupture of a tank valve during tests	Propulsion of the valve towards a pipe connected to a vessel	Hole in the pipe => leaked liquefied gas caught fire => BLEVE of the vessel => propulsion of 1/3 of the tank against the base of a sphere on a neighbouring property while knocking back the 3rd and 4th vessels
2000	Morocco - Casablanca	Urban and road transport: Explosion of a tanker truck refueling 2 butane vessels	Formation of 3 large fragments: the rear half of the bottom was blasted towards a tank 100 m away, a fully unwound ferrule was propelled a few dozen meters away, and the front half of the bottom was propelled towards the front of the truck 40 m away	A pipe connecting the two vessels being refueled was ripped out

Figure 5: Examples of fragment-generating accidents – Consequences of the fragments propelled to nearby entities [BARPI]

2.2 General definition

In everyday language, a shock is a “violent interaction between two separate entities that leads to sudden behaviour changes”. In other words, it is violent contact between two bodies.

In mechanics, we use both “shock” and “impact” when one solid enters into contact with another solid. This phenomenon is of a dynamic nature and is complex to study. It generates, in each of the structures involved, high-amplitude mechanical effects of very short duration, as well as a sudden variation in their velocity.

2.3 Classification proposed by Eibl: Soft impact / Hard impact

[Eibl 1987] and the Euro-International Concrete Committee [CEB 1988] suggested a classification in which the impact of a projectile on a target can be represented by an equivalent mass-spring system. The behaviour of the whole is governed by the following differential equations:

$$\begin{cases} m_1 \frac{d^2 x_1}{dt^2} + k_1 [x_1(t) - x_2(t)] = 0 \\ m_2 \frac{d^2 x_2}{dt^2} + k_1 [x_1(t) - x_2(t)] + k_2 x_2(t) = F(t) \end{cases}$$

where m_1 : projectile mass, k_1 : stiffness of the associated spring
 m_2 : target mass, k_2 : stiffness of the associated spring

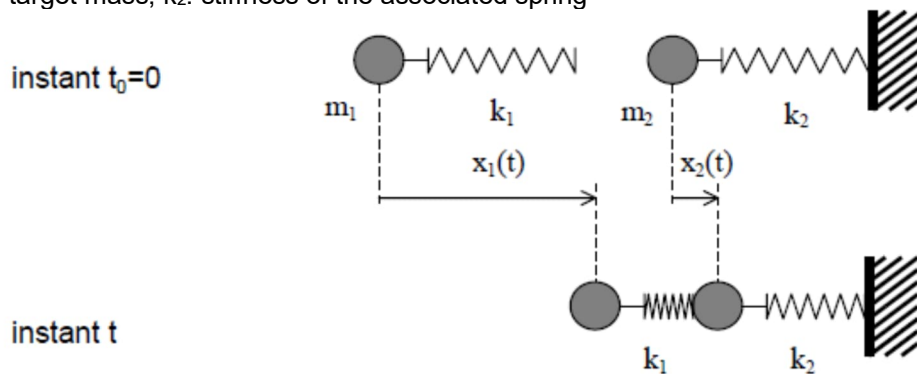


Figure 6: Mass-spring system associated with the modelling of the impact of a projectile [Koechlin 2007]

If the displacement of the target is low compared to the projectile, then $x_1(t) \gg x_2(t)$ the movement equations become:

$$\begin{cases} m_1 \frac{d^2 x_1}{dt^2} + k x_1(t) = 0 \\ m_2 \frac{d^2 x_2}{dt^2} + k_2 x_2(t) = F(t) \end{cases}$$

The problem is then decoupled. It is possible to start by resolving the first equation then, by laying down $F(t)=k_1 x_1(t)$ for example, to deduce $F(t)$ and finally calculate the target’s response using the second equation [Koechlin 2007].

When the projectile’s behaviour can be decoupled from that of the target’s, the shock is qualified by [Eibl 1987] as a mild shock. In the cases where the equations cannot be decoupled, the shock is then qualified as a strong shock or impact.

This classification is quite interesting as it offers a problem-solving method for processing mild shocks, intuitively defined as a soft projectile that crashes into a hard target. It is, for example, traditionally used to translate the impact of an aircraft on a reinforced concrete structure. Life-size trials have proven that, for this type of impact, the projectile is completely crushed and the target’s displacements and distortions are low compared to those of the aircraft [Sugano 1993]. However, it does not properly take into account hard impacts where a rigid projectile penetrates a less rigid target, or when the projectile crushes against a soft but resistant target.

2.4 Unified shock characterisation suggested by Koechlin

[Koechlin 2007] puts forward another classification using a criterion based on the materials' properties and in particular their rupture thresholds. It can be used to characterise any type of shock, regardless of the target's geometry (thickness).

The target's rupture threshold σ_c is compared to that of the projectile σ_p . This determines whether the target will resist the impact. **If the target resists and the projectile is crushed, the shock is qualified as mild; when the projectile penetrates the target, the shock is qualified as strong.**

According to Riera's formula, written as force during the initial shock, the target subjected to impact by a projectile crashing at a speed of V_0 is subjected to a force with two components: one derived from the material, the other from the speed equal to:

$$\sigma = \sigma_p + \rho_p V_0^2$$

where σ_p is the projectile's breaking stress, ρ_p the projectile's density, and V_0 is the projectile's speed.

The limit between hard impact and soft impact is supposedly reached when σ_c , the breaking stress of the material from which the target is made, equal's Riera's force, that is:

$$\frac{\sigma_p}{\sigma_c} + \frac{\rho_p V_0^2}{\sigma_c^2} = 1$$

Riera's formula and therefore the equation above only makes sense if the projectile is crushed (i.e. there is no rebound).

When the projectile rebounds against the target, the issue requires another analysis. The crushing condition (and, therefore, the condition for applying Riera's formula) amounts to saying that the projectile's maximum force exceeds its breaking stress. The crushing condition (or the non-rebound condition) is as follows:

$$V_0 \sqrt{E_p \rho_p} > \sigma_p \text{ where } E_p: \text{ Young modulus for the projectile}$$

Or

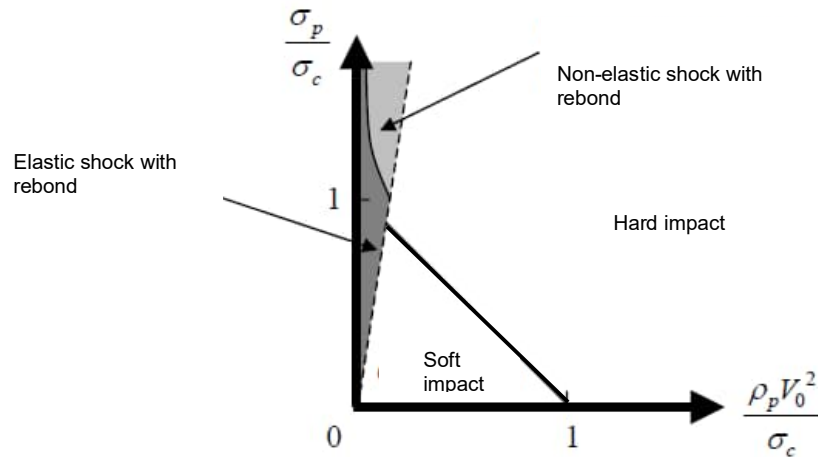
$$\frac{E_p \rho_p V_0^2}{\sigma_p \sigma_c} > \frac{\sigma_p}{\sigma_c}$$

With rebound impacts, it is possible to distinguish between elastic impacts with rebound and non-elastic impacts with rebound. The limit between these two fields is defined by the fact the maximum force in the projectile applied to the target does not reach the target's breaking stress:

$$\frac{E_p \rho_p V_0^2}{\sigma_p \sigma_c} > \frac{\sigma_c}{\sigma_p}$$

This "unified shock characterisation" thus defines 4 fields:

- the soft impact field, namely shocks without rebounds and a deformable projectile;
- the hard impact field: namely non-rebound shocks with a rigid projectile and penetration;
- the elastic shock with rebound field;
- the non-elastic shock with rebound field.



ρ : density (in kg/m^3); σ : breaking stress (in Pa); E : Young's modulus (in Pa)
 c and p indexes: the target and the projectile's index respectively.
 V_0 : the projectile's impact velocity (in m/s)

Figure 7: Shock classification [Koechlin 2007]

The distinction between soft impact and hard impact is a lot more commonly found than the characterisation of shocks with rebound. In reality, the area for shocks with rebound is quite difficult to define. It can be simply said that there exists a field in which the projectile rebounds for low impact velocities. It should be additionally noted that when the speed is high, shocks are generally hard.

Despite the fact this classification does not take into account the projectile's geometry – and appears at first sight to be based on a very localised analysis – it is capable of processing structural shocks.

Finally, the target's geometry has no influence on the proposed classification, which simply establishes the limit between local destruction and complete destruction.

The issue of resistance of structures and other equipment has been and remains vastly studied in the military field, where impact velocities are predominantly supersonic. This is why, as shown in Figure 8, the majority of full-scale or small-scale laboratory trials are within the hard shock field. Meppen is the only one to have conducted trials on soft impacts. An impact trial involving a full-scale aircraft (F-4 Phantom) against a wall has also been conducted.

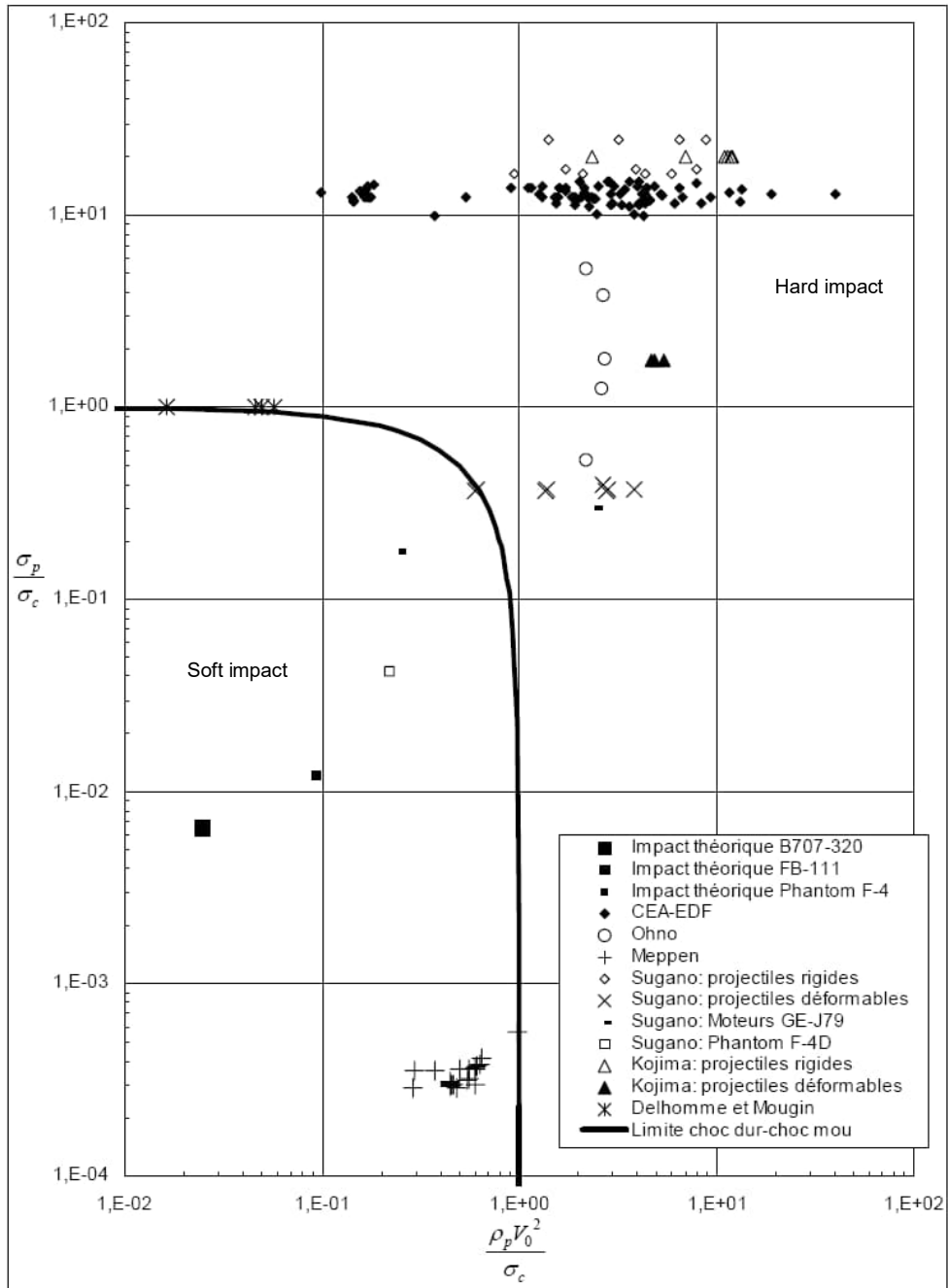


Figure 8: Soft impact / hard impact field [Koechlin 2007]

2.5 Summary

Ineris recommends retaining the definitions and notions of unified shock characterisation suggested by Koechlin, the main principles of which are presented in paragraph **Erreur ! Source du renvoi introuvable.**

2.6 Behaviour of a structure in the event of a projectile impact

A structure's response to projectile impact can be "global" or "local".

- A global response is mainly due to the vibration of the entire structure. Damage appears when the energy transmitted by the impact exceeds the potential energy capacity during deformation.
- The local response is more likely to be in the form of damage localised close to the impact area.

The shorter the duration of impact – as is generally the case in hard impacts – compared to the target's response time, the more decoupled the local and global phenomena will be; the behaviour in close vicinity of the impact is not a result of the entire structure's behaviour and vice versa. Damage processes are independent. For example, studying the shock on an aircraft engine with a purely local analysis seems perfectly pertinent. However, the longer the duration of impact – which is the case for soft impacts – the more the phenomena are coupled. Vibration waves are generated and travel through the structure. It is generally recommended to study both the local behaviour (the local destruction process during perforation) and the consequences of waves spreading throughout the entire structure, i.e. the global behaviour.

The structure's response is dependent on many factors, including the following:

- The projectile's geometric characteristics: diameter, length, shape of the projectile head (flat, round, hemispherical, conical, etc.);
- The projectile's impact velocity;
- The target's geometrical characteristics: thickness and size;
- The target and the projectile's material properties, and especially the projectile's compared to the targets.

2.7 Behaviour of a concrete target against a projectile impact

Certain concrete structures are designed to resist impacts with high kinetic energy levels, such as nuclear plant enclosures.

When a rigid projectile impacts a concrete target, a wave travels through the structure (Refer to Figure 9 a), b) and c)). This is followed by a penetration phase during which the projectile is preceded by a high-pressure area that compresses the material but also tends to eject it. A cratering area tends to form in the impact area at the projectile/target interface. Penetration continues until the projectile stops in the target if the energy required to perforate is not available, a process that can be facilitated by the spalling potentially produced by reflections on the target's rear side.

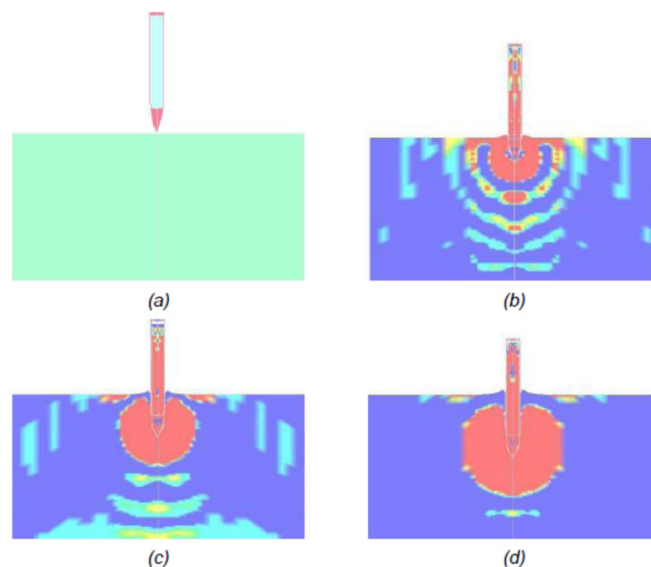


Figure 9: Example of projectile impact on a concrete target

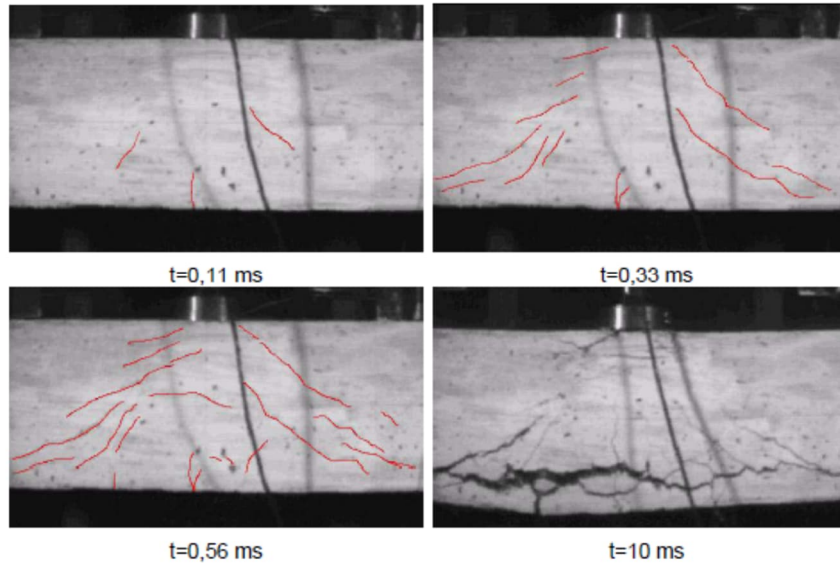


Figure 10: Progression of cracking and formation of the shear cone [May et al. 2005]

The effects of the damage after impact by a projectile on a concrete target can result in 7 major phenomena:

- **Penetration:** a “tunnel” is drilled into the target by the projectile, the length of which is called the “penetration depth”;
- **Cone cracking and plugging:** Formation of a cone-like crack under the projectile and the possible subsequent punching-shear plug.;
- **Spalling:** ejection of target material from the proximal face of the target;
- **Cracking:** radial cracks appear on one or both sides of the target and propagate through its thickness;
- **Scabbing:** ejection of fragment on the rear side;
- **Perforation:** the projectile completely passes through the target with or without residual velocity;
- **Overall structural responses and failures:** Global bending, shear and membrane responses as well as their induced failures throughout the target

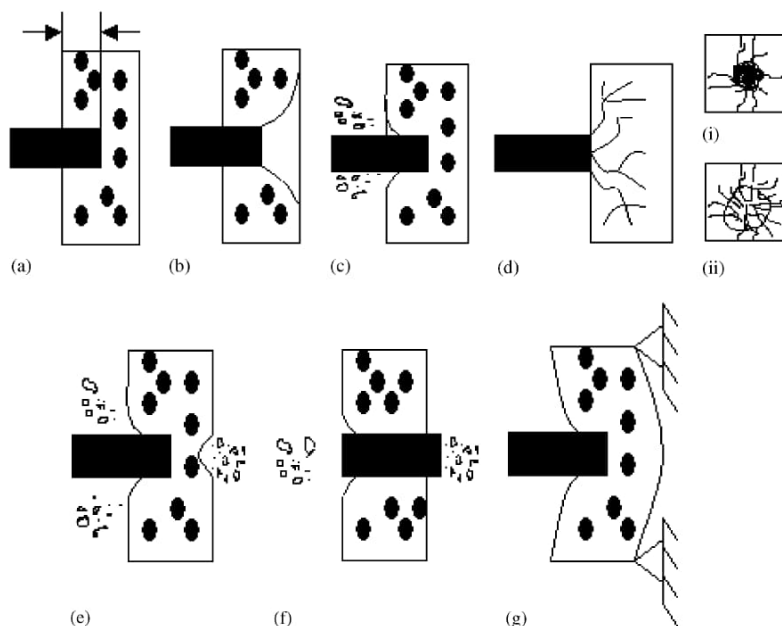


Figure 11. Different effects resulting from impact on a concrete slab: (a) penetration, (b) cone cracking, (c) spalling, (d) Cracks on (i) the front side and (ii) the rear side, (e) scabbing, (f) perforation, and (g) overall target response [Li 2005].

2.8 Behaviour of a steel target against a projectile impact

When it comes to a steel target's local response following impact by a projectile (normal to the target), the damage depends firstly on the target's ductile or fragile behaviour and, on the other hand, on the perforating object's limit of elasticity.

For steel targets with low ductility, the damaging or fracturing methods are generally fragile in nature, as they are for concrete. Spalling is an example of this, predominantly for lower-quality steel.

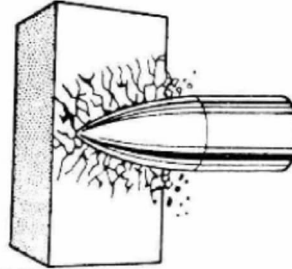


Figure 12: Example of a brittle fracture in a steel target

For ductile metal targets, the mechanisms involved vary depending on the target's thickness. **The first mechanism associated with low thickness is the one that will be the most common in accidental risks.**

- For thin plates, **perforations such as “plugging”** can also occur. For example, punching appears for velocities lower than 1,000 m/s. The projectile shears through the plate exactly like a punch would do. The crater has nearly the same diameter as the projectile. Damage by **petalling** as a result of the bending stress on the target's rear side is also possible. The projectile drives into the target and plastically deforms it. The rupture starts from the penetration axis and extends in many directions, forming petals both on the front and rear side of the target. No secondary fragments are formed.

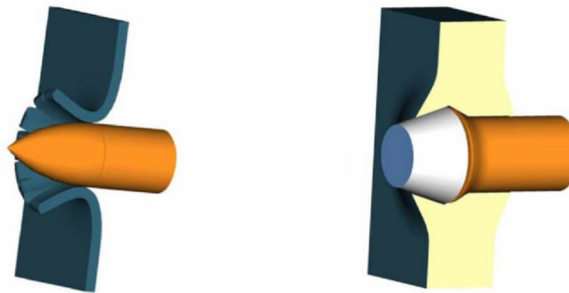


Figure 13: Petalling (left) and punching (right) [IMFRA 2008]

- For thick plates, **penetration and perforation** can occur, as well as the **formation of cone-shaped cracking** due to **shearing (“plugging”)** that can be ejected from the target's rear side.

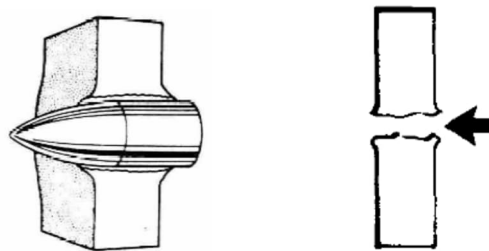


Figure 14: Penetration and perforation [IMFRA 2008]

3 Methods used to calculate the resistance of structures to the impact of projectiles

An industrial site accommodates various facilities. Should a facility explode, the fragments generated and propelled in the vicinity can impact nearby structures such as pipework, atmospheric or pressurised vessels, or supporting structures. They may partially or completely perforate them. Should this occur, these structures may then, in turn, pose a risk for nearby structures and lead to a chain of disastrous events called the domino effect. Accidentology shows that this phenomenon may have caused the rupture of numerous structures and led to numerous casualties.

As previously explained, the risk of destroying such equipment or damaging structural elements following a projectile impact does not only depend on the projectile's impact velocity, but also on its mass and its material properties compared to those of the target.

Numerous research studies have been conducted in order to develop formulas that describe in a simple manner the effects listed in the previous chapter. Most of them mainly focus on establishing formulas that determine performance during penetration, perforation or spalling. These notions are critical when determining the size of protection systems for example. Prediction laws pertaining to these various phenomena can be split into three categories:

- empirical correlations, which are mostly used to assess the effects. They use experimental databases to establish relationships between the depth of penetration / perforation limit thickness and the main calculation parameters (impact velocity, projectile geometry/dimensions, projectile properties, etc.);
- analytical methods generally based on a more or less simplified resolution of the differential equation describing the system;
- numerical methods able to couple a Finite Element (FE) or CFD code (for cases where there is a significant penetration component upon impact) that gives the equivalent force applied to the structure to a Finite Element code that gives the distribution of force within the structure.

3.1 Empirical correlations

Numerous empirical models have been developed in order to translate the local effects of impacts from non-deformable (hard) projectiles on a target, whether it is made of concrete, reinforced concrete or steel. These models are used to assess **damage**, **penetration**, **perforation** or **spalling** (for concrete targets) through different geometric quantities:

- penetration depth x_p : the distance penetrated by the projectile into the target without passing through it;
- perforation limit e_p : minimum target thickness required in order to avoid perforation. This quantity is sometimes characterised by:
 - The ballistic limit for perforation V_p that expresses the minimum speed required to perforate the target. Several definitions exist. Backman and Goldsmith (1978) define it as the mean between the highest speed that generates partial penetration and the lowest speed that generates full penetration (perforation).

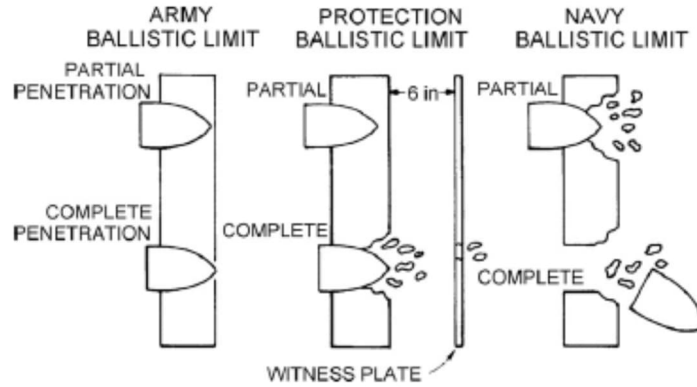


Figure 15: Different definitions of critical perforation speed [Li 2008]

- or the critical perforation energy: the kinetic energy of the projectile required to perforate the target.
- scabbing limit e_s : minimum target thickness in order to avoid scabbing on the rear side.

3.1.1 Generic formulas (concrete/steel) for local impacts

3.1.1.1 THOR equation: supersonic-speed impact

Thor [Thor 1961] provides empirical equations derived from a very large number of perforation trials on metallic and non-metallic targets by steel projectiles. These equations can be used to estimate the ballistic limit for perforation, and the projectile's residual speed in the event of a perforation.

$$V_p = 0.3 \cdot 10^{c_1} (6.1 \cdot 10^4 H_o A)^{c_2} (1.55 \cdot 10^4 M_f)^{c_3} (\sec(\alpha_i))^{c_4}$$

$$V_r = V_0 \left(1 - 10^{c_5} (6.1 \cdot 10^4 H_o A)^{c_6} (1.55 \cdot 10^4 M_f)^{c_7} (\sec(\alpha_i))^{c_8} (3.3 V_0)^{c_9 - 1} \right)$$

As to the perforation limit e_p (in m) of a steel target by a solid steel projectile, it is given by [TNO 2003]:

$$e_p = k (\cos(\alpha_i))^{1.420} \frac{m^{1.063} V_0^{1.103}}{A} \text{ where } k = 1.091 \cdot 10^{-7} \text{ kg}^{-1.063} \cdot \text{m}^{1.897} \cdot \text{s}^{1.103}$$

where V_0 = projectile impacting velocity (m/s)

V_r = residual speed (m/s)

V_p = ballistic limit for perforation (m/s)

H_o = thickness of the target screen (m)

m = projectile mass (kg)

A = average surface area of impact or exposed surface area of the projectile upon impact (m^2).

When the exposed surface area of the projectile upon impact is unknown, the [TNO 2003] suggests keeping A as the following value, which corresponds to the surface area of a standard fragment resulting from a bomb explosion.

$$A = \frac{\pi}{4} \left(\frac{m}{0.645 \rho_{acier}} \right)^{2/3} \text{ where } \rho_{acier}: \text{ steel density}$$

α_i = angle of penetration (compared to the screen's norm) (degrees)

$\text{Sec}(\alpha_i)$ = secant of angle $\alpha_i = 1/\cos(\alpha_i)$

C_1 to C_9 = coefficients based on the nature of the target, specified in the table in Figure 16.

These expressions are only valid for supersonic-speed impacts. Their scope of application is specified in Figure 17; it depends on the nature of the materials constituting the target, its thickness, the projectile's mass and speed as well as the angle of impact of the projectile on the target.

Matériaux (écrans)	C1	C2	C3	C4	C5	C6	C7	C8	C9
Alliages de magnésium	6,349	1,004	- 1,076	0,966	6,904	1,092	- 1,170	1,050	- 0,007
Aluminium (2024T-3)	6,185	0,903	- 0,941	1,090	7,047	1,029	- 1,072	1,251	- 0,139
Fonte	10,153	2,186	- 2,204	2,156	4,840	1,042	- 1,051	1,028	- 0,523
Alliages de titane	7,532	1,325	- 1,314	1,643	6,292	1,103	- 1,095	1,369	- 0,167
Acier traité	7,694	1,191	- 1,397	1,747	4,356	0,674	- 0,791	0,989	- 0,434
Acier doux	6,523	0,906	- 0,963	1,206	6,399	0,889	- 0,945	1,262	- 0,019
Acier dur	6,601	0,906	- 0,962	1,206	6,475	0,889	- 0,945	1,262	- 0,019
Cuivre	14,065	3,476	- 3,687	4,270	2,785	0,678	- 0,730	0,840	- 0,802
Plomb	10,955	2,735	- 2,753	3,590	1,999	0,499	- 0,502	0,655	- 0,818
Tuballoy	14,773	3,393	- 3,510	5,037	2,537	0,583	- 0,603	0,865	- 0,828
Nylon non chargé	5,006	0,719	- 0,563	-0,852	5,816	0,835	- 0,654	0,990	- 0,162
Nylon chargé	7,689	1,883	- 1,593	1,222	4,672	1,144	- 0,968	0,743	- 0,392
Lexan	7,329	1,814	- 1,652	1,948	2,908	0,720	- 0,657	0,773	- 0,603
Plexiglass moulé	6,913	1,377	- 1,364	1,415	5,243	1,044	- 1,035	1,073	- 0,242
Plexiglass étiré	11,460	3,537	- 2,871	2,274	3,605	1,112	- 0,903	0,715	- 0,686
Doron	5,581	0,750	- 0,745	0,673	7,600	1,021	- 1,014	0,917	- 0,362
Verre blindé	6,991	1,116	- 1,351	1,209	3,743	0,705	- 0,723	0,690	- 0,465

Figure 16: Coefficient C_i based on the nature of the impacted target [Thor 1961]

Matériaux (écrans) h (cm)	Epaisseur de l'écran m (kg)	Masse de la projection U_0 (m/s)	Vitesse d'impact ∞_i (degré)	Angle d'impact
Alliages de magnésium	0,13 - 7,62	$0,9710^{-3}$ - $15,610^{-3}$	150-3150	0-80
Aluminium (2024T-3)	0,05 - 5,08	$0,3210^{-3}$ - $15,610^{-3}$	360-3300	0-80
Alliages de titane	0,10 - 3,05	$1,9410^{-3}$ - $15,610^{-3}$	210-3120	0 - 45
Fonte	0,48 - 1,42	$0,9710^{-3}$ - $15,610^{-3}$	330-1830	0-70
Acier traité	0,35 - 1,27	$0,9710^{-3}$ - $15,610^{-3}$	750-2940	0-70
Acier homogène	0,07 - 2,54	$0,3210^{-3}$ - $53,510^{-3}$	180-3600	0-70
Cuivre	0,15 - 2,54	$0,9710^{-3}$ - $15,610^{-3}$	330-3420	0-70
Plomb	0,18 - 2,54	$0,9710^{-3}$ - $15,610^{-3}$	150-3120	0-70
Tuballoy	0,25 - 0,50	$1,9410^{-3}$ - $30,810^{-3}$	1350-3030	0-60
Nylon non chargé	0,05 - 7,62	3.10^{-4} -0,013	90-3000	0-70
Nylon chargé	1,10 - 5,08	3.10^{-4} -0,053	300-3600	0-70
Lexan	0,32 - 2,54	3.10^{-4} -0,015	300-3450	0-70
Plexiglass coulé	2,50-2,80	3.10^{-4} -0,03	60-2850	0-70
Plexiglass étiré	0,13-2,54	3.10^{-4} -0,03	150-3300	0-70
Doron	0,13-3,81	$1,6.10^{-4}$ -0,04	150-3300	0-70
Verre blindé	0,50-4,20	$9,7.10^{-3}$ -0,03	60-3000	0-70

Figure 17: Scope of application for Thor's equations [Thor 1961]

3.1.1.2 “High pressure code” model, De Cox and Saville’s equations: subsonic-speed impacts

The “High Pressure Safety code” (1985, B.G. Cox and G. Saville) [Micado 2002] suggests an empirical formula that calculates an order of magnitude of penetration thicknesses in alloy steel and reinforced concrete for speed ranges below 1,000 m/s.

For fragments with a mass exceeding 1 kg and a length/diameter ratio >1, the thickness of penetration x_p (in mm) is given by:

$$x_p = \frac{CM}{A} \log(1 + 5.10^{-5}V_0^2)$$

where M = projectile mass (kg)

V_0 : projectile impacting velocity (in m/s)

A: visible section of the projectile upon impact (in m²)

C: parameter given in the following table:

Type of material	C
Limestone	7.10 ⁻⁴
unreinforced concrete – compressive ultimate load 15 MN/m ²	10.10 ⁻⁴
unreinforced concrete - compressive ultimate load 22 MN/m ²	6.10 ⁻⁴
unreinforced concrete - compressive ultimate load 40 MN/m ²	3.5.10 ⁻⁴
masonry stone wall	14.10 ⁻⁴
Brick wall	25.10 ⁻⁴
Mild steel	0.5.10 ⁻⁴
Alloy steel	0.3.10 ⁻⁴

Figure 18: Perforation parameter as per the type of material

The table below connects different types of projectiles – which meet the previous conditions – to thicknesses of perforation.

Name	M (kg)	V (m/s)	A (m ²)	Ratio K	e steel (mm)	e concrete (mm)
Valve	35	35	0.06	20.5 x 10 ³	0.45	5.3
Valve	35	100	0.06	58.3 x 10 ³	3.1	36
Reactor fragment	50	150	0.02	375 x 10 ³	25	290
Valve cover plate	40	230	0.02	460 x 10 ³	34	390
Cylinder cover plate	90	150	0.02	675 x 10 ³	44	500

Figure 19: Thicknesses of perforation based on projectile properties [Micado 2002]

When reading the table, we can conclude that there is a multiplying factor of 10 between concrete and steel regarding the thickness of the material in which perforation can be observed.

For small fragments (m <1 kg and L/D ≅ 1), the depth of penetration p (in m) can be calculated using the following formula:

$$x_p = KM^{n_1}V_0^{n_2}$$

where M = fragment mass (in kg)
 V₀ = fragment speed (in m/s)
 K, n₁ and n₂: constants indicated below

Material	K	n1	n2
Unreinforced concrete – compressive ultimate load 35 MN/m ²	18 x 10 ⁻⁶	0.4	1.5
Brick wall	23 x 10 ⁻⁶	0.4	1.5
Mild steel	6 x 10 ⁻⁵	0.33	1.0

Figure 20: Perforation parameter as per the nature of the material

These relationships were established when dimensioning the equipment protection and are correlated with various approaches, including the Petry approach. Unlike the Thor equations, they are generally used for subsonic impact velocities. **They are, de facto, better suited to the issues usually encountered in the industry.**

3.1.1.3 Another formula: Van de Berg's correlation

Van de Berg (1985) [Micado 2002] suggests a **formula that is also suited to industrial issues** and that estimates the perforation power of a projectile in a given target. The penetration depth x_p (in m) is estimated as a function of:

- the projectile impacting velocity;
- the size and the mass of the fragments;
- the nature of the target.

$$x_p = \frac{2}{\rho_c a_c + \rho_p a_p} V_n \Sigma_s \text{ (in m)}$$

where V_n: normal component of the impact velocity (m/s)

Σ_s: mass per projectile surface area unit (kg/m²)

ρ: density (kg/m³) and a: speed of sound assigned to indexes c and p respectively designating the impacted target and the projectile

3.1.2 Concrete targets and local hard impact

Upon impact by a non-deformable (hard) projectile on a concrete or reinforced concrete target, the duration of the penetration process is generally shorter than the response time of the target's overall structure. The effects generated by the impact are thus localised and can result in **penetration, perforation or scabbing**.

Numerous empirical models have been developed in order to translate these local phenomena. This chapter first presents the formulation generally used to describe these phenomena, and then outlines a certain number of these correlations:

- A model developed in the [TM5-1300 1990] and widely used in the military field for projectiles with supersonic impact velocities;
- Models which are more developed for subsonic impact velocities (see Figure 21) and, **de facto, better suited to the problem of domino effects on an industrial site.**

References from empirical models	Nature of the target	Ranges of projectile impact velocities ⁽¹⁾
Petry and modified Petry formulas I and II	Concrete / Reinforced concrete	NR ⁽²⁾
ACE “Army Corps of Engineers” formulas (1943)	Concrete	150 <V ₀ < 900 m/s
Correlations of the NDRC (National Defense Research Committee) adapted by Kennedy (1946-1976) and Degen	Concrete	150 <V ₀ < 900 m/s (Kennedy)
		25 <V ₀ < 310 m/s (Degen)
Correlation of the UKAEA (United Kingdom Atomic Energy Authority) (Barr)	Concrete / Reinforced concrete	25 <V ₀ < 300 m/s
Correlations of the CEA-EDF (Berriaud) (1974)	Reinforced concrete	20 <V ₀ < 200 m/s
Criteria of the R3 Impact Assessment Procedure	Concrete / Reinforced concrete	3<V ₀ <66 m/s

⁽¹⁾: Scope of application of the penetration formulas with regards to the projectile's impact velocity

⁽²⁾: NR: Not reported

Figure 21: Empirical models better suited to industrial issues

All these models adopt the same general formulation outlined below.

3.1.2.1 General formulation

Generally speaking, prediction laws pertaining to the penetration depth can be written as $x_p = f(M, V_0, d, N^*; \rho_c, f_c)$ or in a dimensionless form, as follows:

$$\frac{x_p}{d} = f\left(\frac{MV_0^2}{d^3 f_c}, \frac{M}{\rho_c d^3}, N^*\right)$$

where

M: projectile mass

V₀: initial impact velocity of the projectile

d: projectile diameter

ρ_c: density of the target's concrete

f_c: unconfined compressive stress of the target's concrete

N*: dimensionless parameter: shape factor of the projectile's head

The first term $I = \frac{MV_0^2}{d^3 f_c}$ is called the impact factor (introduced by Haldar et al. (1984)).

The second term $\lambda = \frac{M}{\rho_c d^3}$ corresponds to the $\frac{M}{d^2}$ ratio on a characteristic target area density ρ_cd.

The two dimensionless numbers I and λ define the Johnson damage number commonly used to determine the severity of an impact:

$$\varphi_J = \frac{I}{\lambda} = \frac{\rho V_0^2}{f_c}$$

As the prediction law pertaining to the penetration depth has been given, the perforation limit and scabbing limit are generally determined via a linear or quadratic relation, function of x_p.

In this way, the damage to a given concrete or reinforced concrete target with a thickness of H₀ can be characterised as follows:

- if H₀>e_s the projectile shall remain inside the target with a penetration depth of x_p. The concrete on the rear side shall hold without an elastic regime.
- if e_p<H₀<e_s the projectile penetrates the target and scabbing occurs.
- Finally, if H₀<e_p the missile can perforate the target.

3.1.2.2 TM5-1300 models: projectiles with a supersonic impact velocity

The [TM5-1300 1990] provides empirical formulas for calculating the thickness of penetration of a metal projectile which impacts a **concrete slab** for **supersonic speeds**.

- For a **steel Armor Piercing Fragments** (with a high hardness scale), the projectile's penetration depth in a massive concrete slab (i.e a slab with infinite thickness) is given by:

$$x_p = 4.0 \cdot 10^{-3} (KND)^{0.5} d^{1.1} V_0^{0.9} \text{ if } x_p \leq 2d$$

$$x_p = 4.0 \cdot 10^{-6} KND d^{1.2} V_0^{1.8} + d \text{ if } x_p > 2d \text{ (US)}$$

Where K: penetrability constant $K = \frac{12.91}{f_c}$

$$N = 0.72 + 0.25\sqrt{n - 0.25}$$

f_c in psi, d in inches and V_0 in fps

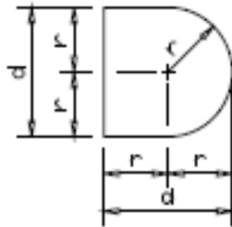
$n = \frac{r}{d}$ where r: hemispherical head radius and d: projectile diameter

D: density: $D = \frac{M_f}{d^3}$; M_f : fragment mass (in oz.)

If the "perforating" projectile has a shape similar to that described in Figure 22, the penetration depth is given by:

$$x_p = \sqrt{\frac{4000}{f_c}} 2.86 \cdot 10^{-3} d^{1.1} V_0^{0.9} \text{ if } x_p \leq 2d$$

$$x_p = \sqrt{\frac{4000}{f_c}} 2.04 \cdot 10^{-6} d^{1.2} V_0^{1.8} + d \text{ if } x_p > 2d \text{ (US)}$$



d: diameter of the projectile's cylindrical section

r: radius of the projectile's hemispherical head

$r = d/2$, $n=2$, $N=0.845$, $D=2976 \text{ oz/in}^3$

Figure 22: Shape of the reference projectile

- For **metal fragments other than armor-piercing**, the penetration depth is given by:

$$x'_p = kx_p \text{ (US)}$$

Where x'_p : maximum penetration in concrete of metal fragments other than armor-piercing fragments

x_p : maximum penetration of armor-piercing fragment

k: constant depending on the nature of the metal constituting the projectile

Nature of the steel	Perforating steel	Mild steel	Lead	Aluminium
k	1.00	0.70	0.50	0.15

The thickness of penetration of a perforating projectile can also be obtained by reading a graph (Figure 23) for a standard concrete target characterised by a strength of 4,000 psi (28 MPa). The penetration depth for a concrete target with a different unconfined compressive stress is given by:

$$x'_p = \sqrt{\frac{4000}{f_c}} x_p \text{ (US)}$$

where x_p : maximum penetration determined by reading the graph for a concrete compressive strength target of 28 MPa

f_c : concrete compressive strength constituting the target

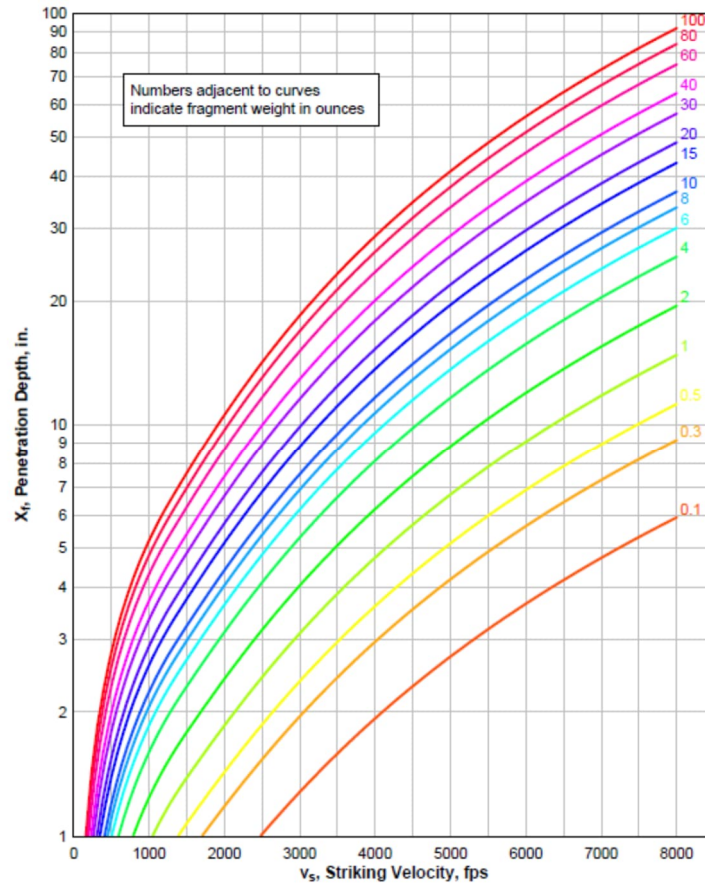


Figure 23: Penetration depth based on the impact velocity and mass of the projectile made of “perforating” steel

- **For any type of steel projectile**

The TM5-1300 also suggests a formula to estimate the perforation limit, in other words the minimum thickness in order to prevent perforation of the target:

$$\frac{e_p}{d} = 1.13 \frac{x_p}{d^{0.9}} + 1.311 \text{ (US)}$$

The residual speed V_r after perforation of a concrete slab with a thickness of H_0 following normal impact by a steel projectile is given by:

$$\frac{V_r}{V_0} = \left(1 - \left(\frac{H_0}{e_p} \right)^2 \right)^{0.555} \text{ (US)}$$

The spalling limit e_s (i.e. minimum thickness to prevent spalling) is given by:

$$\frac{e_s}{d} = 1.215 \frac{x_p}{d^{0.9}} + 2.12 \text{ (US)}$$

3.1.2.3 *Petry and modified Petry formulas (1910)*

The “modified” Petry formulas are amongst the most commonly encountered in literature written in English. They are based on the oldest empirical prediction law found in literature, and originally developed in 1910. They can predict the thickness of penetration of a projectile in a concrete or reinforced concrete target of infinite thickness.

$$\frac{x_p}{d} = k \frac{M}{d^3} \log_{10} \left(1 + \frac{V_0^2}{19,974} \right) \text{ (SI)}$$

where $k = 0.0795K_p$

K_p : penetrability coefficient. It can be incorporated to the Petry formula in two different ways in order to generate the modified Petry formulas I and II.

- Modified Petry formula I: the K_p coefficient is a constant (function of the percentage of reinforcement of the structure in question);

	Non-reinforced concrete	Reinforced concrete: normal reinforcement rate	Reinforced concrete: specially reinforcement rate
K_p	0.00799	0.00426	0.00284

Figure 24: Penetrability coefficient

- Modified Petry formula II: the K_p coefficient is a function of the concrete's compressive strength (reference curve: K_p is a decreasing exponential function of the compressive strength).

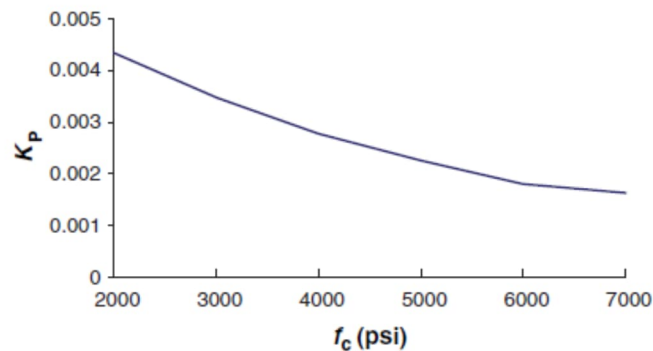


Figure 25: Evolution of K_p depending on the concrete's compressive strength f_c (Li [2005])

Using the previous formulas, Amirikian [Li 2005] suggested the following formulas in order to predict the perforation and scabbing limit.

- perforation thickness: $\frac{e_p}{d} = 2 \frac{x_p}{d}$
- scabbing thickness: $\frac{e_s}{d} = 2.2 \frac{x_p}{d}$

3.1.2.4 ACE "Army Corps of Engineers" formulas (1943)

These formulas are based on the experimental results obtained in 1943 by the American army. They focus more on **non-reinforced concrete** and are valid for **speeds ranging from 150 m/s to 900 m/s** and relatively **high projectile masses** (exceeding 180 kg). Furthermore, they do not take into account the shape of the projectile.

		Scope of application
penetration depth	$\frac{x_p}{d} = \frac{3.5 \cdot 10^{-4} M}{\sqrt{f_c} d^3} d^{0.215} V_0^{1.5} + 0.5$ (SI)	150 < V_0 < 900 m/s 10.5 < f_c < 56 MPa 2.5 < D < 40 cm 180 < M < 1120 kg
perforation limit	$\frac{e_p}{d} = 1.23 + 1.07 \frac{x_p}{d}$ if $1.35 < \frac{x_p}{d} < 13.5$ or $3 < \frac{e_p}{d} < 18$	
scabbing limit	$\frac{e_s}{d} = 2.28 + 1.13 \frac{x_p}{d}$ if $0.65 < \frac{x_p}{d} < 11.75$ or $3 < \frac{e_s}{d} < 18$	

3.1.2.5 Correlations of the NDRC (National Defense Research Committee) adapted by Kennedy (1946, 1966) and Degen

Drawing from the formulas developed by the ACE and additional experimental data, in 1946 the NDRC developed another law to predict the depth of penetration in a concrete target (generally not reinforced).

In 1966 Kennedy suggested an adjustment to this formulation as well as the formulations suggested by the ACE in order to predict perforation limit and scabbing limit [Li 2005]. Like for the ACE model, they focus more on **non-reinforced concrete** and are valid for **impact velocities ranging from 150 m/s to 900 m/s**. However, **they take into account the shape of projectile's nose**.

Shape of the projectile's impacting part (projectile nose)	Flat	Hemispherical	Blunt	Very sharp
Associated shape factor N*	0.72	0.84	1.0	1.14

Figure 26: Shape factor associated with the projectile's impacting part

		Scope of application
penetration depth	$G = 3.8 \cdot 10^{-5} \frac{N^* M}{d \sqrt{f_c}} \left(\frac{V_0}{d} \right)^{1.8} \text{ (SI)}$ $\frac{x_p}{d} = 2G^{0.5} \text{ if } G \geq 1, \frac{x_p}{d} = G + 1 \text{ if } G < 1,$	150 < V ₀ < 900 m/s 10.5 < f _c < 56 MPa 2.5 < D < 40 cm 180 < M < 1120 kg
perforation limit	$\frac{e_p}{d} = 3.19 \frac{x_p}{d} - 0.718 \left(\frac{x_p}{d} \right)^2 \text{ if } \frac{x_p}{d} \leq 1.35 \text{ or } \frac{e_p}{d} \leq 3$ $\frac{e_p}{d} = 1.32 + 1.24 \frac{x_p}{d} \text{ if } 1.35 < \frac{x_p}{d} < 13.5 \text{ or } 3 < \frac{e_p}{d} < 18$	
scabbing limit	$\frac{e_s}{d} = 7.91 \frac{x_p}{d} - 5.06 \left(\frac{x_p}{d} \right)^2 \text{ if } \frac{x_p}{d} \leq 0.65 \text{ or } \frac{e_s}{d} \leq 3$ $\frac{e_s}{d} = 2.12 + 1.36 \frac{x_p}{d} \frac{e_s}{d} = 2.12 + 1.36 \frac{x_p}{d} \text{ if } 0.65 < \frac{x_p}{d} < 11.75 \text{ or}$ $3 < \frac{e_s}{d} < 18$	

Degen [Li 2005] suggests, from statistical analyses and experimental data, another formulation for the perforation and scabbing limit for subsonic impact velocities.

		Scope of application
perforation limit	$\frac{e_p}{d} = 2.2 \frac{x_p}{d} - 0.3 \left(\frac{x_p}{d} \right)^2 \frac{e_p}{d} = 2.2 \frac{x_p}{d} - 0.3 \left(\frac{x_p}{d} \right)^2 \text{ if } \frac{x_p}{d} \leq 1.52 \frac{x_p}{d} \leq 1.52$ $\text{or } \frac{e_p}{d} \leq 2.65$	25.0 < V ₀ < 311.8 m/s 28.4 < f _c < 43.1 MPa 0.10 < d < 0.31 m 0.15 < H ₀ < 0.61 m

3.1.2.6 Correlation of the UKAEA (United Kingdom Atomic Energy Authority)

Barr [Li 2005] suggests an adjustment of the formulas developed by the NDRC for **smaller impact velocities ranging from 25 to 300 m/s** falling more within the **field of industrial accidents** than the military sector.

		Scope of application
penetration depth	$G = 3.8 \cdot 10^{-5} \frac{N^* M}{d \sqrt{f_c}} \left(\frac{V_0}{d} \right)^{1.8} \text{ (SI)}$ $\frac{x_p}{d} = 0.275 - (0.07656 - G)^{0.5} \text{ if } G \leq 0.0726,$ $\frac{x_p}{d} = (4G - 0.242)^{0.5} \text{ if } 0.0726 \leq G \leq 1.0605,$ $\frac{x_p}{d} = G + 0.9395 \text{ if } G \geq 1.0605$	25 < V ₀ < 300 m/s 22 < f _c < 44 MPa 5,000 < $\frac{M}{d^3}$ < 200,000 kg/m ³
perforation limit	$V_p = V_a \text{ if } V_a \leq 70 \text{ m/s}$ $V_p = V_a \left(1 + \left(\frac{V_a}{500} \right)^2 \right) \text{ if } V_a > 70 \text{ m/s}$ <p>where</p> $V_a = 1.3 \rho_c^{\frac{1}{6}} k_c^{\frac{1}{2}} \left(\frac{p H_0^2}{\pi M} \right)^{\frac{2}{3}} (r + 0.3)^{\frac{1}{2}} \left(1.2 - 0.6 \left(\frac{c_r}{H_0} \right) \right) \text{ if } 0.12 < \frac{c_r}{H_0} < 0.49$ $V_a = 1.3 \rho_c^{\frac{1}{6}} k_c^{\frac{1}{2}} \left(\frac{p H_0^2}{\pi M} \right)^{\frac{2}{3}} (r + 0.3)^{\frac{1}{2}} \text{ if } \frac{c_r}{H_0} > 0.49$ <p>k_c : k_c=f_c if f_c<37 MPa k_c=37 MPa if f_c≥37 MPa H₀: target thickness p: perimeter of the projectile's section r: percentage of steel reinforcement c_r: spacing between the reinforcements</p>	Flat-headed projectile 11 < V ₀ < 300 m/s 22 < f _c < 52 MPa 150 < $\frac{M}{p^2 H_0^3}$ < 10 ⁴ kg/m ³ 0.33 < $\frac{H_0}{p/\pi}$ < 5.0 0 < r < 0.75%
scabbing limit	$\frac{e_s}{d} = 5.3 \left(0.55 \frac{x_p}{d} - \left(\frac{x_p}{d} \right)^2 \right)^{0.33} \text{ if } \frac{x_p}{d} \leq 0.22$ $\frac{e_s}{d} = 5.3 \left(\left(\frac{x_p}{2d} \right)^2 + 0.0605 \right)^{0.33} \text{ if } 0.22 \leq \frac{x_p}{d} \leq 2.0$ $\frac{e_s}{d} = 5.3 \left(\frac{x_p}{d} + 0.9395 \right)^{0.33} \text{ if } \frac{x_p}{d} \geq 2.0$	29 < V ₀ < 238 m/s 26 < f _c < 44 MPa 3,000 < $\frac{M}{d^3}$ < 222,200 kg/m ³

The above formulas take account of the shape of the projectile's nose through an N* factor, the values of which can be found in the table below.

Shape of the projectile's impacting part	Flat	Hemispherical	Round	Very sharp
Associated shape factor N*	0.72	0.84	1.0	1.14

Figure 27: Shape factor associated with the projectile

The estimation of the perforation velocity is only valid for flat-headed projectiles. For other types of projectiles, Barr [Li 2005] believes that the formula can conservatively estimate the penetration. For projectiles with a hemispherical head and a diameter approximately equal to the thickness of the target, or for those with a sharper shape, the speed of near-perforation is approximately 30% higher compared to that of a flat-headed projectile with the same mass and dimensions.

3.1.2.7 Correlations of the "Commissariat à l'Energie Atomique" (Atomic Energy Commission or CEA) and "Electricité de France" (EDF) (1974)

As part of a research program launched in 1974, the CEA-EDF conducted experimental trials where projectile masses, dimensions and impact velocities varied as well as the compressive strength and nature of the reinforcement in the targets. From these trials, Berriaud [Li 2005] developed a correlation that estimates the ballistic limit as well as the perforation limit of a **reinforced concrete slab** with a thickness of H_0 and **density of reinforcements** ranging from **100 to 250 kg/m³** for projectile velocities.

		Scope of application
ballistic limit	$V_p = 1.3 \rho_c^{1/6} f_c^{1/2} \left(\frac{d H_0^2}{M} \right)^{2/3} \text{ (SI)}$	20 < Vo < 200 m/s 30 < f _c < 45 MPa
perforation limit	$\frac{e_p}{d} = 0.82 \frac{M^{1/3} V_0^{2/3}}{\rho_c^{1/3} f_c^{1/2} d^{2/3}} \text{ (SI)}$	100 kg/m ³ < density of reinforcements < 250 kg/m ³ 0.5 < $\frac{D}{H_0}$ < 1.5

Sliter [Sliter 1980] examined the reliability of this prediction law through a considerable number of trials that revealed **good adequacy between the prediction of ballistic speeds and the experimental data**.

Thereafter, Fullard [Fullard 1991] amended this law by taking into account the influence of the reinforcement rate r_d :

$$V_p = 1.3 \rho_c^{1/6} f_c^{1/2} \left(\frac{p H_0^2}{\pi M} \right)^{2/3} (r_d + 0.3)^{1/2} \text{ (SI)}$$

with p as the perimeter of the missile cross-section.

3.1.2.8 Criteria of The R3 Impact Assessment Procedure

The previous formulas are generally valid for relatively substantial subsonic – or even supersonic – impact velocities. [Reid and Wen 2001] and the [BNFL 2003] suggest formulas in order to translate the **local penetration, perforation and scabbing effects of a "hard" impact on a concrete or reinforced concrete target for range of speeds under 60 m/s**.

These formulations are highly developed as they take into account the shape of the projectile, whether or not the concrete is reinforced, and the presence of potential reinforcements (percentage and spacing).

- penetration depth:

$$\frac{x_p}{d} = \frac{2 N^* M V_0^2}{\pi 0.72 \sigma_t d^3} \text{ (SI)}$$

$$\text{with } \sigma_t = 4.2 f_c + 135 \cdot 10^6 + (0.014 f_c + 0.45 \cdot 10^6) V_0 \text{ (SI)}$$

Shape of the projectile's impacting part	Flat	Hemispherical	Round	Very sharp
Associated shape factor N*	0.72	0.84	1.0	1.13

This formula is valid providing the following assumptions are respected:

- $3 < V_o < 66.2$ m/s
- $50 < d < 600$ mm
- $35 < M < 2,500$ kg
- $0 < \frac{x_p}{d} < 2.5$

Thereafter, they are expressed in terms of the projectile's threshold or critical kinetic energy.

		Scope of application
Critical kinetic energy to cause perforation	$\frac{E_p}{\eta \sigma_t d^3} = -0.00506 \left(\frac{H_0}{d}\right) + 0.01506 \left(\frac{H_0}{d}\right)^2 \text{ if } 0 < \frac{H_0}{d} \leq 1$ $\frac{E_p}{\eta \sigma_t d^3} = -0.01 \left(\frac{H_0}{d}\right) + 0.02 \left(\frac{H_0}{d}\right)^3 \text{ if } 1 \leq \frac{H_0}{d} < 5$ $\frac{E_p}{\sigma_t d^3} = \frac{\pi}{4} \left(\left(\frac{H_0}{d}\right) - 3.0\right) \text{ if } \frac{H_0}{d} \geq 5$	$0 < V_o < 427$ m/s $22 < d < 600$ mm $1 < M_r < 2,622$ kg $19.9 < f_c < 78.5$ MPa $0 < r < 4\%$
Critical kinetic energy to cause scabbing	$\frac{E_s}{\eta \sigma_t d^3} \frac{N^*}{0.72} = -0.005441 \left(\frac{H_0}{d}\right) + 0.01386 \left(\frac{H_0}{d}\right)^2 \text{ if } 0.5 \leq \frac{H_0}{d} < 5$ $\frac{E_s}{\sigma_t d^3} \frac{N^*}{0.72} = \frac{\pi}{4} \left(\left(\frac{H_0}{d}\right) - 4.3\right) \text{ if } \frac{H_0}{d} \geq 5$	$50.8 < H_0 < 640$ mm $0 < \frac{x_p}{d} < 2.5$
Critical kinetic energy to cause cone cracking	$\frac{E_c}{\eta \sigma_t d^3} = -0.00031 \left(\frac{H_0}{d}\right) + 0.00113 \left(\frac{H_0}{d}\right)^2 \text{ if } 0 < \frac{H_0}{d} \leq 2$ $\frac{E_c}{\eta \sigma_t d^3} = -0.00325 \left(\frac{H_0}{d}\right) + 0.00130 \left(\frac{H_0}{d}\right)^3 \text{ if } 2 \leq \frac{H_0}{d} < 5$ $\frac{E_c}{\sigma_t d^3} = \frac{\pi}{4} \left(\left(\frac{H_0}{d}\right) - 4.7\right) \text{ if } \frac{H_0}{d} \geq 5$	-

In all last three formulas, the η parameter is determined by:

$$\eta = \begin{cases} \frac{3}{8} \left(\frac{d}{C_r}\right) r_t + 0.5 & \text{if } \left(\frac{d}{C_r} < \sqrt{\frac{d}{d_r}}\right) \\ \frac{3}{8} \left(\sqrt{\frac{d}{d_r}}\right) r_t + 0.5 & \text{if } \left(\frac{d}{C_r} \geq \sqrt{\frac{d}{d_r}}\right) \end{cases}$$

with

$$\begin{cases} d_r: \text{diameter of the target's steel reinforcements} \\ C_r: \text{spacing between the reinforcements} \\ r_t = 4r \text{ with } r \text{ as the percentage of reinforcement in the target: } r = \frac{\pi d_f^2}{4H_0 C_r} \end{cases}$$

It must be emphasised that fracturing caused by cone cracking is an important local fracture where the reinforced concrete enclosure contains gas or pressurised liquid.

3.1.2.9 Comparison of empirical correlations

Models for supersonic impact velocities, and other models for subsonic velocities

The empirical models proposed above are amongst the most commonly used models. The models developed by the TM5-1300 can be used to study impacts for supersonic speeds. The others are valid for subsonic impact velocities. Amongst them, the Petry, ACE and NDRC formulations are widely recognised for the sizing of protective structures.

Influence of the shape factor

The majority of these formulations (with the exception of Petry's formulas) take into account the influence of the shape factor of the projectile's nose when determining penetration depth. However, there is no unity when it comes to defining it, and one has to be vigilant when it comes to the different coefficients used. Li and Chen [Li and Chen 2003] underline the need to define a unique shape factor. This aspect, associated with the fact that formulas can sometimes be dependent on the units in which they have been established, can be challenging when conducting parametric analyses or when comparing models with each other or with experimental results.

Taking into account the reinforcement rate

Furthermore, in the majority of the correlations studied, the target's reinforcement rate is rarely considered. However, the modified Petry formulations I and II suggest an overall approach. Those suggested by Fullard, extension of the CEA-EDT formula, by the UKA/KEA or by the "R3 Impact Assessment Procedure", can also be used to take into account this parameter in a more refined manner, and in particular to predict perforation.

A limited scope of application

The proposed models are derived from experimental data. As a result, they are only valid for a precise domain that matches that of the trials. However, various comparisons of empirical formulas in which the projectile's parameters are set (for example Kennedy: 45.45 kg projectile with a 15.24 cm diameter and a rounded nose or Berriaud: 30 to 50 kg projectile [Yankelevsky 1997] and [Li 2005]) show that the **modified NDRC model can be considered as a representative formula of the empirical formulas in order to predict the thickness of penetration of a rigid projectile for speeds below 300 m/s.** It tends to average the results derived from empirical models. This is also the case for perforation (see Figure 28 and Figure 29).

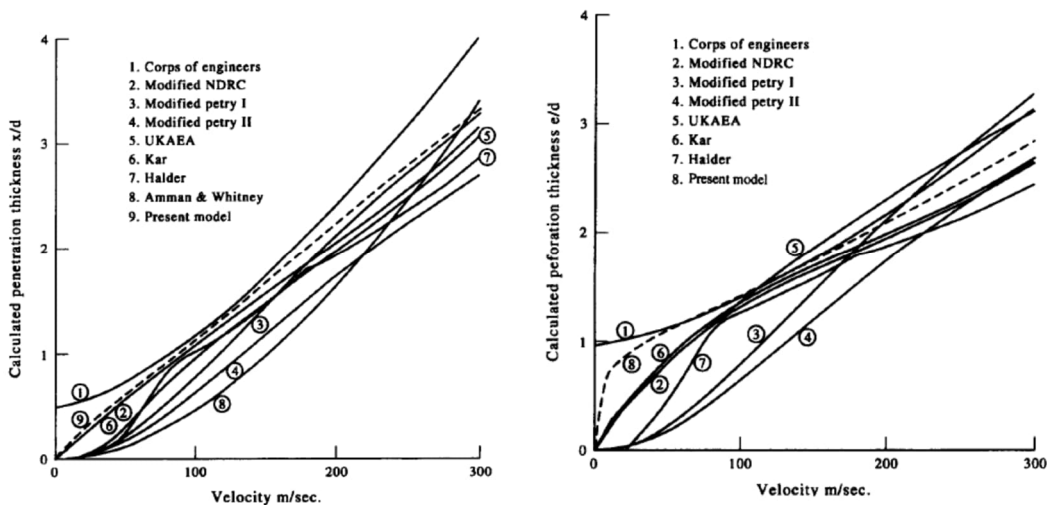


Figure 28: Comparison between different empirical models [Yankelevsky 1997]

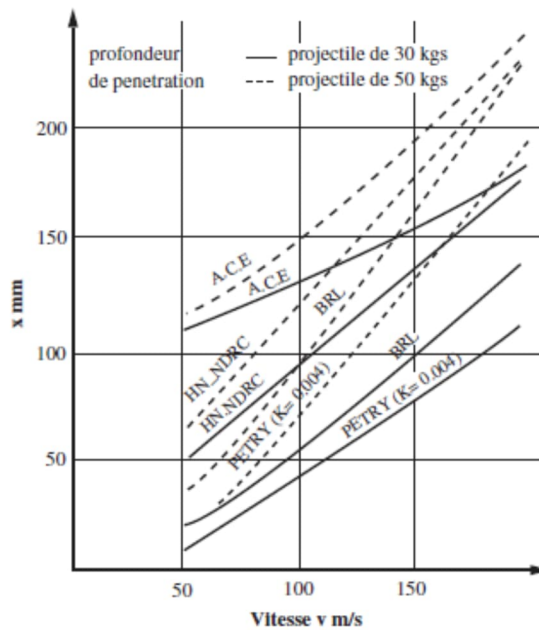


Figure 29: Comparison of different empirical models [Li 2005]

The ARLCD-SP-84001 manual of the US Department of Defense Explosive Safety Board recommends using the **NDRC's modified formulas for penetration and perforation but also to translate scabbing.**

The US Air Force's ESL-TR-87-57 manual promotes the **modified approach developed by the NDRC for penetration and the ACE's formulas for calculating perforation and scabbing.**

The most recent manual, that of the British Army, recommends using the **UKAEA formulas to calculate penetration and scabbing and the ones developed by the CEA and EDF for perforation.**

Most of these formulations are used in the upper region of the subsonic speed domain for which they give consistent results.

However, for **lower speeds**, important differences appear (Figure 28 and Figure 29). This is why the **use of other formulas, such as those suggested by the "R3 Impact Assessment Procedure"** – based on the work conducted by the UMIST that aims at predicting all the phenomena – is preferred. These formulas are valid for low to intermediate impact velocities (60 m/s). For small velocities, the penetration depth can also be calculated using semi-analytical models developed by Li and Chen [Li and Chen 2003] which are detailed in Chapter **Erreur ! Source du renvoi introuvable.**

3.1.3 Steel target and local hard impact

Numerous empirical models have been developed in order to translate the local effects of the impact of a non-deformable (hard) projectile on a steel target. In most cases, the impact is considered as normal to the target.

As is the case for concrete targets, the purpose of this chapter is to present the empirical models commonly used to assess penetration and perforation:

- A model widely used in the military field (formulas from the TM5-1300) for projectiles with supersonic impact velocities;
- Models further developed for impacts with subsonic impact velocities on steel plates;
- Models particularly suited to impacts against atmospheric or pressurised vessel walls or pipes at subsonic speed.

The last two categories are the best suited to the issue of domino effects on industrial sites.

3.1.3.1 Wall impacts: projectiles with a supersonic impact velocity

The [TM5-1300 1990] provides empirical formulas for calculating the **thickness of penetration of a metal projectile that impacts a mild steel plate for supersonic speeds.** These formulas are given for a normal impact and depend on the relative hardness of the projectile compared to the plate.

- **For Armor Piercing steel fragments penetrating mild steel plates**, the penetration depth is given by:

$$x_p = 2.35 \cdot 10^{-5} M_f^{0.33} V_o^{1.22} \text{ (SI)}$$

where M_f : projectile mass (kg)

V_o : the projectile's impact velocity (in m/s) (SI)

- **For mild steel fragments penetrating mild steel plates**, the penetration depth is given by:

$$x'_p = k x_p \text{ (SI)}$$

With k : parameter depending on the nature of the metal the projectile is made from

Nature of the steel	Perforating steel	Mild steel	Lead	Aluminium
K	1.00	0.70	0.50	0.15

The thickness of penetration can also be obtained by reading graphs for two configurations out of those suggested for the formulas:

- Armor Piercing steel fragments.
- Mild steel fragments.

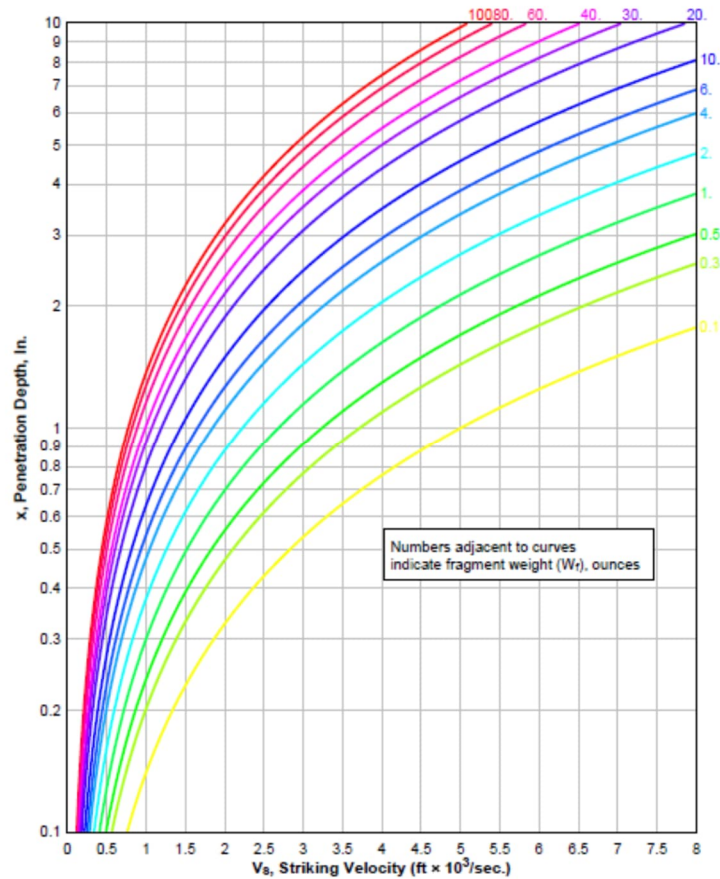


Figure 30: Penetration depth based on the impact velocity and mass of an armor piercing steel fragment

The TM5-1300 also suggests calculating the V_r residual speed after perforation of a steel plate with a thickness of H_0 following normal impact by a projectile that is also made of steel.

$$\frac{V_r}{V_0} = \frac{\left(1 - \left(\frac{V_c}{V_0}\right)^2\right)^{\frac{1}{2}}}{\left(1 + \frac{H_0}{d}\right)}$$

Where V_0 : projectile's impact velocity

d: diameter of the projectile's cylindrical section

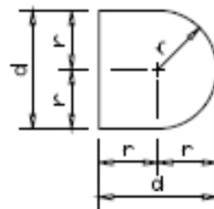


Figure 31: Shape of the reference projectile

The speed can be calculated using the previous equations by replacing the penetration depth with the H_0 thickness of the plate under consideration.

3.1.3.2 Wall impacts: projectile with a subsonic impact velocity

Below are the most commonly used empirical formulas that translate the perforation of metal plates following a subsonic impact. **This speed domain is typically that of the fragments generated during an industrial explosion.**

The criterion is given by determining the critical perforation energy defined by:

$$E_{cr} = f(d, H_0, w, L, \sigma_u, \beta)$$

where

d: projectile diameter

L: length of the projectile,

H_0 : thickness of the target plate

w: length of the target plate

σ_u : traction stress of the steel in the target plate

β : shape factor for the projectile's head

If the projectile's E_c kinetic energy upon impact is greater than the E_{cr} critical perforation energy, the target will perforate.

It is generally expressed in a dimensionless manner:

$$\frac{E_{cr}}{\sigma_u d^3} = g\left(\frac{H_0}{d}, \frac{w}{d}, \frac{L}{d}, \beta\right)$$

or as

$$\frac{E_{cr}}{\sigma_u d^3} = g\left(\frac{H_0}{d}, \frac{w}{d}, \frac{L}{d}\right) \text{ for a given shape of projectile head.}$$

On a practical level, the $\frac{L}{d}$ ratio does not explicitly appear in the formulations but can be used to define the scope of application. As a result, the critical perforation energy depends mostly on two dimensionless parameters $\frac{H_0}{d}$ (the most influential parameter) and $\frac{w}{d}$.

The formulas can be classified in 2 categories, depending on the shape of the projectile's head:

- projectile with conical or hemispherical nose;
- projectile with flat nose.

3.1.3.2.1 Projectiles with conical / hemispherical nose

Reference	Formulas	Scope of application	
		Projectiles	Targets
Othe et al. (1982)	$\frac{E_{cr}}{\sigma_u d^3} = \left(\frac{\sigma_r}{\sigma_u}\right) \left(\frac{H_0}{d}\right)^3 \left(1 + 2.9 \left(\tan\left(\frac{\beta}{2}\right)\right)^{2.1}\right)^{1.5} \text{ for } \frac{H_0}{d} > d_e = \left(1 + 2.9 \left(\tan\left(\frac{\beta}{2}\right)\right)^{2.1}\right)^{-1}$ $\frac{E_{cr}}{\sigma_u d^3} = \left(\frac{\sigma_r}{\sigma_u}\right) \left(\frac{H_0}{d}\right)^{1.5} \text{ for } \frac{H_0}{d} \leq d_e = \left(1 + 2.9 \left(\tan\left(\frac{\beta}{2}\right)\right)^{2.1}\right)^{-1}$ $\sigma_r = 3 \cdot 10^8 \text{ kgf/m}^2$	Conical projectiles 25 < V _o < 180 m/s d _e > d	H ₀ = 7-38 mm, 0.08 < $\frac{H_0}{d}$ < 0.45, $\frac{w}{H_0}$ > 39, 4.7 < $\frac{w}{d}$ < 11.4 σ _u = 490 MPa
SRI modified by Corbett and Reid (1993)	$\frac{E_{cr}}{\sigma_u d^3} = 3.285 \left(\frac{H_0}{d}\right)^2 + 0.0077 \left(\frac{H_0}{d}\right) \left(\frac{w}{d}\right)$	Hemispherical projectiles 100 < V _o < 250 m/s	0.2 < $\frac{H_0}{d}$ < 0.6, 31 < $\frac{w}{H_0}$ < 83
Neilson modified by Corbett and Reid (1993)	$\frac{E_{cr}}{\sigma_u d^3} = 0.9 \left(\frac{H_0}{d}\right)^{1.7} \left(\frac{w}{d}\right)^{0.6}$	Hemispherical projectiles 100 < V _o < 250 m/s	1 < H ₀ < 25 mm, 0.2 < $\frac{H_0}{d}$ < 0.6, 31 < $\frac{w}{H_0}$ < 83

3.1.3.2.2 Projectile with flat nose

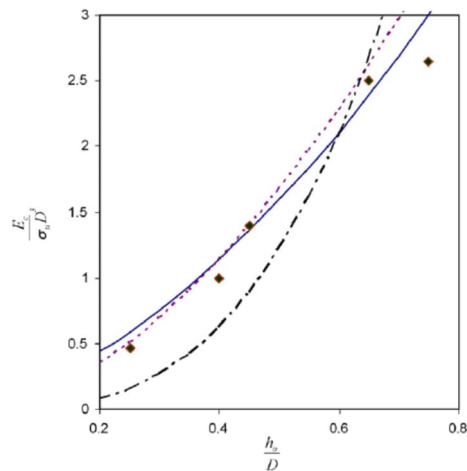
Reference	Formulas	Scope of application	
		Projectiles	Targets
Wen and Jones (1992)	$\frac{E_{cr}}{\sigma_u d^3} = 2 \left(\left(\frac{\pi}{4} \right) \left(\frac{\sigma_y}{\sigma_u} \right) \left(\frac{H_0}{d} \right)^2 + \left(\frac{\sigma_y}{\sigma_u} \right) \left(\frac{w}{d} \right)^{0.21} \left(\frac{H_0}{d} \right)^{1.27} \right)$	Vo < 20 m/s Flat or round head	$0.4 < \frac{H_0}{d} < 1.6$, $25 < \frac{w}{H_0} < 100$ $\frac{w}{d} < 40$, $340 < \sigma_u < 440$ MPa
SRI (1963)	$\frac{E_{cr}}{\sigma_u d^3} = 4.150 \left(\frac{H_0}{d} \right)^2 + 0.097 \left(\frac{H_0}{d} \right) \left(\frac{w}{d} \right)$	21 < Vo < 122 m/s $10 < \frac{L}{d} < 50$	$0.1 < \frac{H_0}{d} < 0.6$, $0.002 < \frac{H_0}{L} < 0.05$ $3 < \frac{w}{d} < 8$
Neilson (1993)	$\frac{E_{cr}}{\sigma_u d^3} = 1.38 \left(\frac{H_0}{d} \right)^{1.68} \left(\frac{w}{d} \right)^{0.61} \text{ if } 4 < \frac{w}{d} < 22.0$ $\frac{E_{cr}}{\sigma_u d^3} = 9.09 \left(\frac{H_0}{d} \right)^{1.68} \text{ if } \frac{w}{d} \geq 22.0$	10 < Vo < 100 m/s $\frac{L}{d} > 13$ (long projectiles), 32 < d < 85 mm 1 < M < 20 kg	$0.14 < \frac{H_0}{d} < 0.64$, $4 < \frac{w}{d} < 22$ (or $\frac{w}{d} = 22.0$) $1 < H_0 < 25$ mm
BRL (1968)	$\frac{E_{cr}}{\sigma_u d^3} = \frac{1.44 \cdot 10^9}{\sigma_u} \left(\frac{H_0}{d} \right)^{1.5}$	57 < Vo < 270 m/s $1.25 < \frac{L}{d} < 8$	$0.1 < \frac{H_0}{d} < 1.0$, $8 < \frac{w}{d} < 35$ $315 < \sigma_u < 500$ MPa

3.1.3.2.3 Comparison of the empirical models and Ineris model

Whatever the projectile's shape, the **scope of application of each of the proposed formulas is relatively specific** and corresponds to the field for which the experimental data has been obtained.

Projectiles with hemispherical nose:

Few empirical formulas exist to predict the critical perforation energy of a steel plate by a conical or hemispherical-headed projectile. **The adjustments to the SRI or Neilson models by Corbett and Reid (1993) or Othe's formula [Li 2008] are the most commonly used when it comes to subsonic speeds.** By comparing these formulas with the experimental data obtained by Corbett and Reid (1993), Othe's formula appears to be more conservative for values of $\frac{H_0}{d} < 0.6$.



{curve designation is: (----) modified SRI (Corbett and Reid, 1993), (---) modified Neilson (Corbett and Reid, 1993), (.....) Othe ($\beta = 65^\circ$) (Othe et al., 1982), (◆) experimental data (Corbett and Reid, 1993)};

Figure 32: Comparison of the prediction of Corbett et Reid's (1993) empirical models and experimental data with a hemispherical-headed projectile

Projectiles with flat nose:

This typical projectile model is more suited to the issue of projectile impacts following domino effects on an industrial site.

According to the "R3 Impact Assessment Procedure", **BRL formulas are recommended for compact projectiles ($L/d < 10$), whereas the SRI or Neilson's formulas are better suited to longer projectiles ($L/d > 10$).** Furthermore, for low-velocity (< 20 m/s) high-mass impacts, the studies conducted by [Corbett et Reid 1996] show that Wen and Jones' formula generates good predictions.

However, it should be underlined that each of the developed models is only valid for a restricted scope of application. Furthermore, the BRL model contains experimental parameters that do not take into account the mechanical properties of the materials composing the projectile and the plate. The SRI and Neilson models – despite being a function of the target's maximum breaking stress – appear to overestimate the critical perforation energy required and, as a result, underestimate – and rather considerably so in some cases – the thickness of penetration for a given projectile kinetic energy [Mebarki et al. 2007].

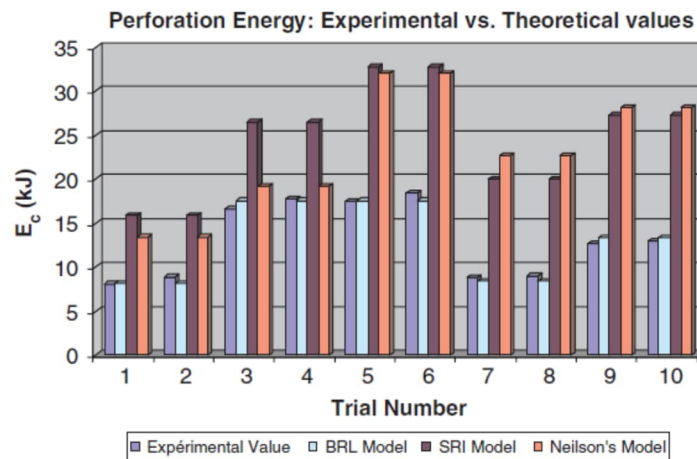


Figure 33: Comparison of the theoretical and experimental results on the series of trials conducted by Lepareux (1989) [Mebarki et al. 2007]

Ineris model

Ineris and the Mechanical Laboratory of the University of Marne la Vallée suggest an **alternative model of penetration** [Mebarki et al. 2007]. This simplified model, **particularly suited to risk assessments in industrial environments**, can be used to estimate the penetration depth following impact by a cylindrical projectile on a steel plate. It takes into account the mechanical properties of the materials composing the projectile and the target, as well as the projectile's geometric and kinematic properties. Furthermore, it **estimates the penetration depth regardless of the angle formed by the projectile and the target**.

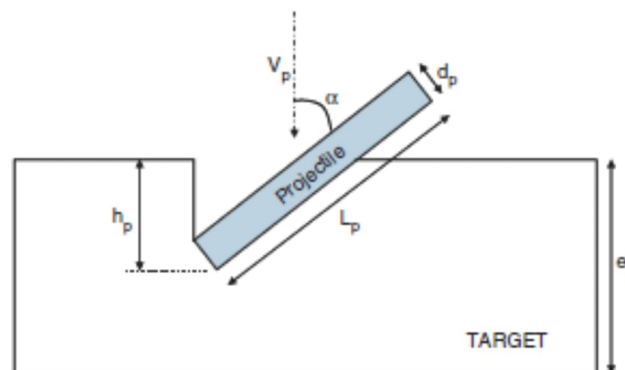


Figure 34: Penetration of a cylindrical projectile in a steel target [Mebarki et al. 2007]

It is based on the following assumptions and principles:

- the projectile is assumed to be rigid and does not distort upon impact. This assumption is valid if the target is made of a material that is less rigid than the projectile;
- the material composing the target is assumed to have plastic behaviour;
- upon impact, the projectile's penetration to thickness x_p plasticises the target – with an effective volume of V_{eff} – around the contact area. The dissipated energy E_{pl} is thus defined as equal to the projectile's kinetic energy E_c upon impact.

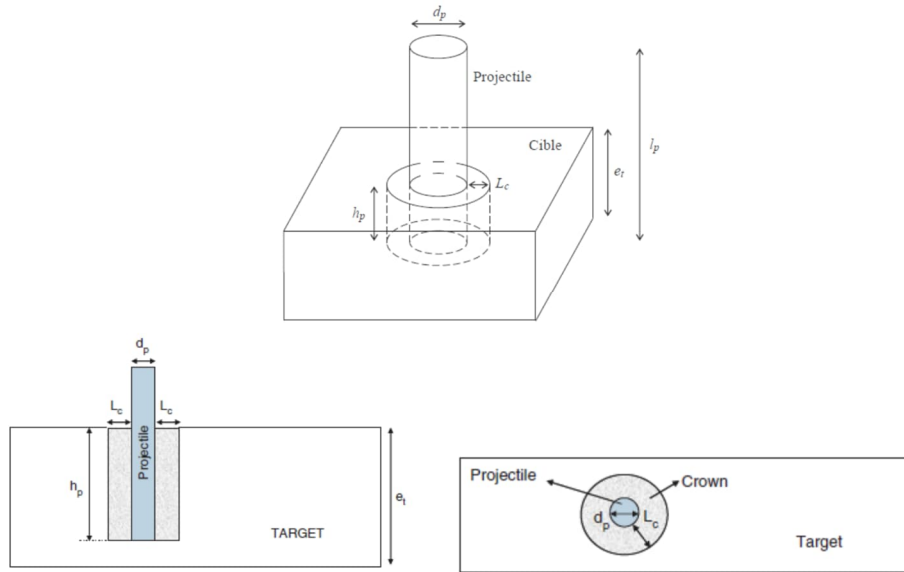


Figure 35: Normal impact (tilt angle of 0) of a cylindrical projectile on a steel target: plasticised effective volume around the contact area [Mebarki et al. 2007]

As a result, the thickness of penetration of a projectile arriving with a tilt angle of α on a steel plate is given by:

If $\alpha = 0$	$x_p = \frac{1}{\pi d_p} \left(\frac{E_c}{f_u \epsilon_u} \right)^{\frac{2}{3}} \text{ with } E_c = \frac{1}{2} m_p v_p^2 \quad (\text{SI})$
If $\alpha \neq 0$	$x_p = \frac{-d_p \cos \alpha + \sqrt{(d_p \cos \alpha)^2 + 4 \tan \alpha \left(\frac{E_c}{f_u \epsilon_u} \right)^{\frac{2}{3}} \frac{1}{\pi}}}{2 \tan \alpha} \quad (\text{SI})$

Where f_u :

stress of the material composing the target

breaking

ϵ_u : maximum deformation of the material composing the target

d_p : projectile diameter

m_p : projectile mass

v_p : projectile speed

x_p : penetration depth of the projectile

Additionally, this model is associated with an error model so as to take into account mechanical simplifications and the inherent disparities and uncertainties pertaining to the model's different entry parameters (the projectile's material, geometric, speed and mass parameters).

The comparison with several trial series ([Lepareux, 1989], [Neilson, 1985] and [Borvik, 2003] or [Bless et al. 1978] and [Bukharev et al., 1995] for a non-zero tilt angle) reveals that, **in most cases, the proposed model yields theoretical results consistent with the experimental results.** It appears to be very efficient for the Lepareux series, where the predicted depths of penetration are close to the ones observed (see Figure 36) (the relative error is below 6.3%). It is also relatively consistent with the observations for the Borvik (2003) trials (see Figure 37) [Mebarki et al. 2007].

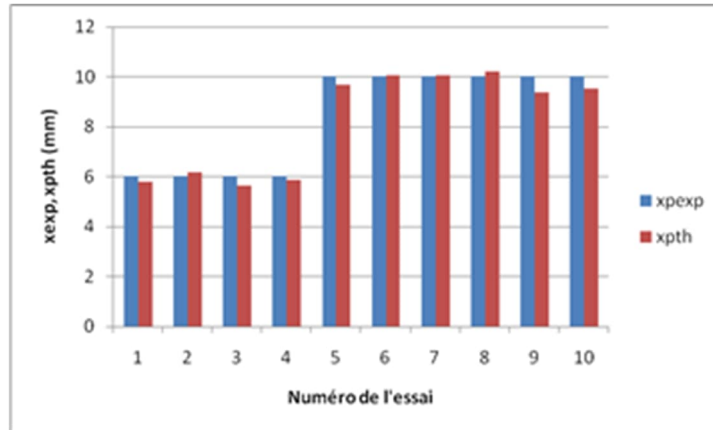


Figure 36: Comparison between the Lepareux (1989) experimental depths of penetration and the Ineris model

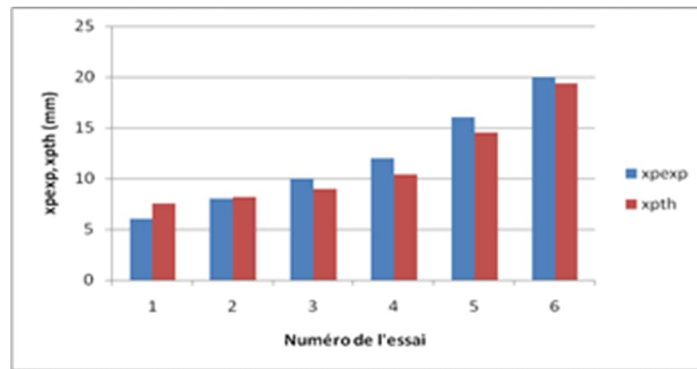


Figure 37: Comparison between the Borvik (2003) experimental depths of penetration and the theoretical Ineris model

3.1.3.3 Impact of vessel walls or walls of liquefied gas spheres

The formulas presented above can be used to translate the penetration and/or perforation of targets such as metal plates. **In order to study the behaviour of the walls of steel atmospheric or pressurised storage vessels, HSE [HSE 1998] suggests perforation criteria that are more specific and particularly suited to the issue of domino effects generated by fragments on industrial sites.**

The models are based on the determination of the projectile's threshold or critical kinetic energy that leads to the perforation of the target and are summarised in the table below.

Two cases are considered:

- Case no. 1: the projectile side with the largest width impacts the target "normally"; in doing so, the impact surface area is relatively big. With a conservative approach, the fragment is considered as a blunt object.
- Case no. 2: the projectile side with the smallest width impacts the target "normally"; the impact surface area is very localised, the generated stress concentrations are a lot higher than those caused by a blunt object.

Atmospheric vessel		
Case	Formulas	Scope of application
1	High Pressure Safety Code model (1975): $E_p = \frac{1}{2} M_f V_p^2 = 1.5 \cdot 10^9 D^3 \left(\frac{H_0}{D} \right)^{1.41}$	$M_f < 50$ kg
	For a 15 mm-thick mild steel plate, $E_p = AM_f + B$ with $A = 1.564 \times 10^3$ and $B = 3.06 \times 10^5$	$50 < M_f < 1,000$ kg $0.384 < E_p < 1.87$ MJ
2	High Pressure Safety Code model where $D=5H_0$ (Impact surface diameter equal to 5 times the thickness of the atmospheric vessel (Pietersen's assumption)): $E_p = 1.5 \cdot 10^9 \cdot 5^{1.59} (H_0)^3$	$M_f < 50$ kg
	For a 15 mm-thick mild steel plate, the maximum speed of perforation is given by: $V_p = \sqrt{\frac{130000}{M_f}}$	$50 < M_f < 1,000$ kg

Pressurised vessel		
Case	Formulas	Scope of application
1	Miyamoto model $E_p = \frac{1}{2} M_f V_p^2 = 2.9 \cdot 10^9 H_0^{1.5} D^{1.5}$	$3 < M_f < 50$ kg, $7 < H_0 < 38$ mm, $25 < V_0 < 170$ m/s, $66 < D < 160$ mm
	For a 15 mm-thick hardened steel plate, $E_p = AM_f + B$ where $A = 2.148 \times 10^3$ and $B = 4.80 \times 10^5$	$50 < M_f < 1,000$ kg $0.587 < E_p < 2.628$ MJ
2	Miyamoto model where $D=5H_0$ (Impact surface diameter equal to 5 times the thickness of the atmospheric vessel): $E_p = 32.4 \cdot 10^9 H_0^3$	$3 < M_f < 50$ kg, $7 < H_0 < 38$ mm, $25 < V_0 < 170$ m/s
	For a 15 mm-thick hardened steel plate, the maximum speed of perforation is given by: $V_p = \sqrt{\frac{218 \cdot 10^3}{M_f}}$	$50 < M_f < 1,000$ kg

Where M_f : mass of the sphere with an equivalent volume (in kg)

D: diameter of the sphere's propelled surface (in m)

H_0 : target thickness (in m)

E_p : critical perforation kinetic energy (in J)

V_p : ballistic limit (in m/s)

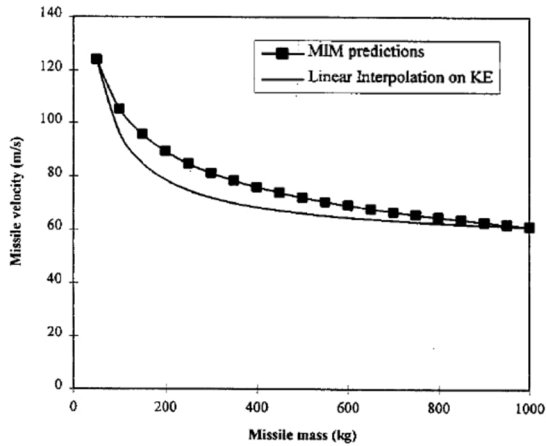


Figure 38: Maximum speed of penetration of a 15 mm-thick mild steel plate (Case no. 1)

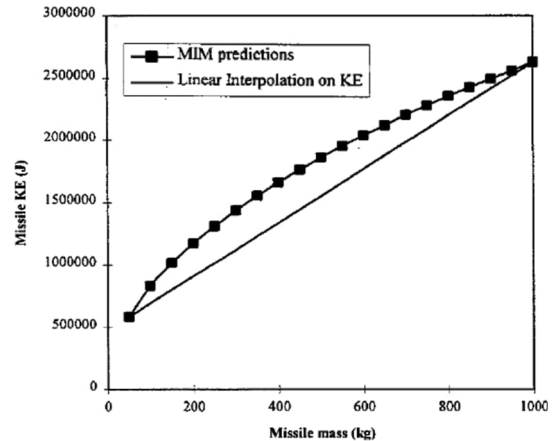


Figure 39: Critical kinetic energy of perforation of a 15 mm-thick hardened steel plate (Case no. 1)

3.1.3.4 Pipework impacts

In order to determine whether **steel pipework is perforated following an impact by projectiles at subsonic speed with a mass of less 50 kg**, HSE [HSE 1998] recommends the SCI (Steel Construction Institute) model (1992). The critical perforation energy is given by:

$$\frac{E_p}{D^3} = A_u \left(\frac{H_0}{D}\right)^{1.7} \left(\frac{D}{D_r}\right)^{0.5} \quad (\text{SI})$$

- where
- M_f : missile mass (in kg)
 - D : missile diameter (in m)
 - H_0 : target thickness (in m)
 - D_p : pipework diameter (in m)
 - A_u : empirical constant 8×10^9 (J/m³)
 - E_p : critical perforation energy (in J)

This relationship is only valid under the following considerations:

- $7 < H_0 < 18$ mm
- $4 < M_f < 50$ kg
- $25 < D < 170$ mm
- $D_p = 150$ mm

This formula is similar to the one proposed by Neilson [Corbett and Reid 1996] valid for a V_0 impact velocity ranging from 80 m/s to 170 m/s.

For **projectiles with a M_f mass ranging from 50 kg to 1,000 kg**, HSE [HSE 1998] suggests another formulation based on the linear interpolation of the critical perforation kinetic energy curve according to the mass between the following two pairs: (50 kg; 90 m/s) and (1,000 kg; 50 m/s).

$$E_p = AM_f + B \quad (\text{SI}) \quad \text{where } A = 1.102 \cdot 10^3 \text{ and } B = 1.474 \times 10^5$$

$$50 < M_f < 1,000 \text{ kg}$$

$$0.202 < E_p < 1.250 \text{ MJ}$$

The corresponding impact velocity, called the ballistic perforation, is given by:

$$V_p = \sqrt{2A + \frac{B}{M_f}} \quad (\text{SI}) \quad \text{where } 50 < M_f < 1,000 \text{ kg}$$

$$50 \text{ m/s} < V_p < 90 \text{ m/s}$$

3.1.4 Limits of the empirical models

The impact of a projectile on a target and the resulting local effects are complex mechanical phenomena. This is why empirical models – based on the use of experimental data by “curve fitting” methods – are widely used. Numerous design codes use them, in particular to determine protective barriers.

However, these models have some drawbacks:

- the non-homogeneous dimensional form of the formulas makes it difficult to conduct parametric analyses or to compare experimental results with analytical predictions as well as to compare experimental results to one another;
- the formulas' scope of application is limited; due to a lack of understanding of the mechanisms governing the phenomena involved, these formulas are only valid in the subject matter for which the experimental data has been obtained;
- the definitions of projectile shape factors – the head in particular – given in most formulas, including for concrete targets, remain ambiguous and introduce uncertainties when estimating the local effects caused by the impact.

3.2 Analytical methods

3.2.1 General information

Schematically speaking, the theory pertaining to the impact of solids can be represented by four main models [Faik 2000]:

- classic mechanics, which applies conservation of momentum and kinetic energy to predict speeds after impact. It makes an assumption about the impact of rigid bodies (instantaneous contact). The dissipation of energy upon impact depends on the nature of the impact, which itself is a function of the coefficient of restitution. This coefficient can vary from 0 (full plastic impact) to 1 (full elastic impact). The models based on this principle cannot be used to describe the contact force or stresses generated by the impact between two bodies.
- the propagation of an elastic wave, which dissipates the impact energy far from the impact area. If the energy that has been transformed into vibrations is a large proportion of the energy involved, it must be taken into account in a model. Generally speaking, this effect is weak when the duration of contact is high compared to the weakest natural frequency of each of the bodies.
- contact mechanics, which is used to determine the stresses resulting from the impact of bodies. It is an extension of the work conducted by Hertz pertaining to static contacts. Unlike the previous models, it takes into account the relative indentation produced on the bodies close to the point of impact, and therefore the duration of contact which has a non-null value.
- plastic deformation, which must be taken into account when it goes beyond the scale of the contained deformation. This phenomenon is generally associated with high impact velocities. Amongst the theories that describe it are those pertaining to the propagation of a plastic wave and the hydrodynamic theory on the behaviour of solid bodies.

3.2.2 Models of target global responses

These models take into consideration the impact of a projectile on a structure from the perspective of an application force for a certain time.

Regarding soft impacts (deformable projectile against a rigid target), [Eibl, 1987] suggests that the behaviour of the projectile can be decoupled from that of the target. As a result, the problem can be solved by **estimating the impact force $F(t)$** using, for example, the **[Riera, 1968] approach**, then by determining the response of the target subjected to this impact force. According to Riera, the impact force $F(t)$, which crushes perpendicularly on a rigid target, can be broken down into two periods: one relating to the buckling of the projectile, the other derived from the inertia of the mass:

$$F = P_f(x(t)) + \mu(x(t)) V^2(t)$$

Where P_f : projectile buckling force

μ : projectile linear density;

V : speed of the projectile at impact;

$x(t)$ the crushed distance (from the nose of the projectile).

Other, more complete, expressions of impact force have been suggested [Abbas 1993]. For example, [Sugano 1993] suggests the following formulation:

$$F = P_f(x(t)) + \alpha\mu(x(t)) V^2(t)$$

where α is a coefficient of effective mass on impact ranging between 0.5 and 1.

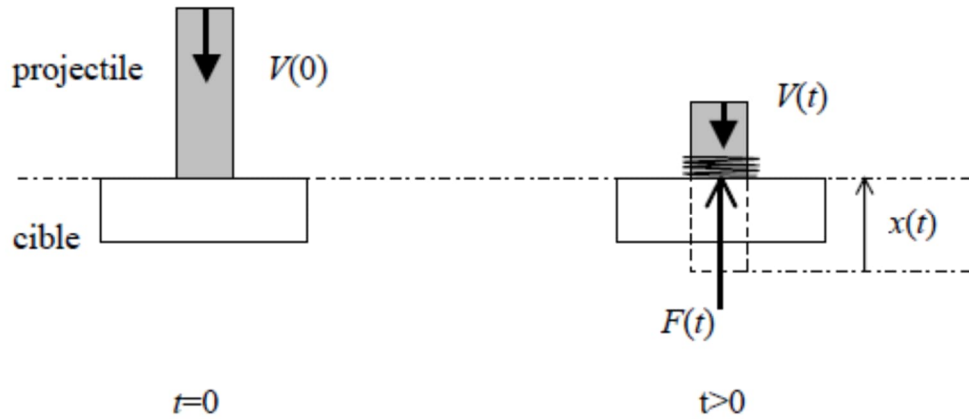


Figure 40: Modelling of a soft impact: determining the impact force [Riera 1968]

Concerning soft impacts, Eurocode NF EN 1991-1-7 of February 2007 supplies an impact resistance criterion when the following condition is met:

$$\frac{1}{2}M_f V_0^2 \leq F_0 y_0$$

Where:

- F_0 is the structure's plastic resistance, in other words the maximum value of the static force of impact;
- y_0 is the structure's deformation capacity, in other words the displacement of the point of impact that the structure can tolerate.

The highest speed that the target can bear must therefore verify:

$$V_0 \leq \sqrt{\frac{2F_0 y_0}{M_f}}$$

In this case, the kinetic energy is completely transformed into plastic deformation.

A similar approach has been used since 1980 when it comes to the resistance of concrete structures – nuclear plants in particular – to aircraft impacts [Meder 1982] and [USAEC 1974] by taking into account a dynamic amplification factor (DAF).

Regarding hard impacts, Eurocode NF EN 1991-1-7 of February 2007 suggests the following equations:

$$F = V_0 \sqrt{kM_f}$$

where

V_0 : speed of the object upon impact;

K : equivalent rigidity of the object;

M_f : mass of the impacting object.

Where:

$$F \Delta t = M_f V_0 \text{ and } \Delta t = \sqrt{\frac{M_f}{k}}$$

and:

$$k = \frac{EA}{L} \text{ and } M_f = \rho_c EA$$

Where L is the length of the impacting object, ρ_c its density, A the cross section's area and E the elastic modulus. Δt represents the duration of impact.

3.2.3 Response model translating a localised hard impact

3.2.3.1 Model based on the resistance force upon penetration

The approach taken consists of resolving the movement equation of a rigid projectile that is governed by Newton's second law:

$$M_f \frac{dV}{dt} = -F_R \text{ with the following initial conditions:}$$

$$\begin{cases} V = V_0 \\ X = 0 \end{cases} \text{ at } t=0$$

where $V = \frac{dx_p}{dt}$

x_p is the thickness of penetration and V the speed of the projectile.

M_f = projectile mass

F_R : penetration resistance, also called force due to projectile/target material interaction during impact

It is generally given in the form of a binomial function of the instantaneous projectile velocity:

$$F_R = F_R(V) = \alpha + \beta V + \gamma V^2.$$

It can also be expressed as a polynomial function with two variables: $F_R = F_R(x_p; V) = g\left(\frac{x_p}{d}\right) f(V)$

The rigid projectile's dynamic movement during impact and penetration can then be analytically determined in order to estimate the projectile's thickness of penetration. These models can also include the shape of the projectile's head.

Poncelet or Wen (2001) [Li 2008] suggested the following expressions:

$$F_R = A(a + bV^2) \text{ (Poncelet)}$$

$$F_R = A(\alpha f_c + \beta \sqrt{\rho f_c} V) \text{ (Wen)}$$

In these formulas, A represents the cross-sectional area of the projectile nose, the coefficients (a , b , α , β) are constants to be determined which are related to the projectile's geometry and the target's mechanical properties. These constants are, for the most part, determined on an experimental basis.

One of the most used force/penetration analytical models for concrete targets is based on the [Forrestal 1994] models, subsequently improved by [Li and Chen 2003] for projectiles of various shapes. This force-penetration model is based on cavity expansion theory and breaks down penetration into two periods.

First, it takes into consideration a crater penetration phase where F_R is expressed as follows:

$$F_R = c \cdot x_p \text{ for } \frac{x_p}{d} < k \text{ with } c = \frac{\pi d}{4k} \frac{(N^* \rho_c V_0 + S f_c)}{\left(1 + \left(\frac{\pi k d^3}{3 M_f}\right) N^* \rho_c\right)}$$

Secondly, it takes into consideration a tunnel area where:

$$F_R = \pi \left(\frac{d}{2}\right)^2 (S \cdot f_c + N^* \cdot \rho_c \cdot V_0) \text{ for } \frac{x_p}{d} \geq k$$

x_p : penetration depth

S : target penetrability factor $S = 72.0 f_c^{-0.5}$

d : projectile diameter

M_f = projectile mass

f_c : unconfined compressive strength of concrete

N^* : shape factor of the missile: $0 \leq N^* \leq 1$:

Shape factor	Conditions
$N^* = \frac{1}{3\psi} - \frac{1}{24\psi^2}$	Ogival-headed projectile, $\psi = \frac{R}{d}$ R : ogive radius; $0 < N^* < 0.5$
$N^* = \frac{1}{1 + 4\psi^2}$	Conical-headed projectile, $\psi = \frac{h}{d}$, h : length of the projectile's nose; $0 < N^* < 1$
$N^* = 1 - \frac{1}{8\psi^2}$	Spherical-headed projectile, $\psi = \frac{R_s}{d}$, R_s : Spherical head radius; $0.5 < N^* < 1$
$N^* = 0.5$	Hemispherical-headed projectile
$N^* = 1$	Flat-headed projectile

$k = 0.707 + \left(\frac{l}{d}\right)$ where l = length of the projectile for $\frac{x_p}{d} < 5$, $k = 2$ pour $\frac{x_p}{d} \geq 5$

Resolving the movement equation leads to a thickness given by:

For $\frac{x_p}{d} \geq 0.5$:

$$\begin{cases} \frac{x_p}{d} = \sqrt{\frac{\left(1 + \frac{k\pi}{4N}\right) 4k}{1 + \frac{l}{N}} \frac{I}{\pi}} & \text{for } \frac{x_p}{d} < k \\ \frac{x_p}{d} = \frac{2}{\pi} N \ln \left(1 + \frac{1 + \frac{l}{N}}{1 + \frac{k\pi}{4N}} \right) + k & \text{for } \frac{x_p}{d} \geq k \end{cases}$$

For $\frac{x_p}{d} \leq 0.5$:

$$\frac{x_p}{d} = 1.628 \left(\frac{\frac{4k}{\pi} I}{1 + \frac{l}{N}} \right)^{1.395}$$

with $I = \frac{1}{s} \left(\frac{M_f V_0^2}{d^3 f_c} \right)$ and $N = \frac{1}{N^*} \left(\frac{M_f}{\rho_c d^3} \right)$

All these formulas have been validated by a large panel of experimental trials for projectiles of various shapes with different impact velocities.

3.2.3.2 Multi-step models

The majority of the models presented assume one fracture mechanism takes precedence over the others: penetration for example. However, impact is a complex phenomenon that involves a combination of various fracture mechanisms (cratering, formation of a cone of cracks, spalling, fragmentation...). This can particularly be observed on targets of median thickness where the predominating perforation process evolves with the penetration of the target by the projectile [Woodward 1984].

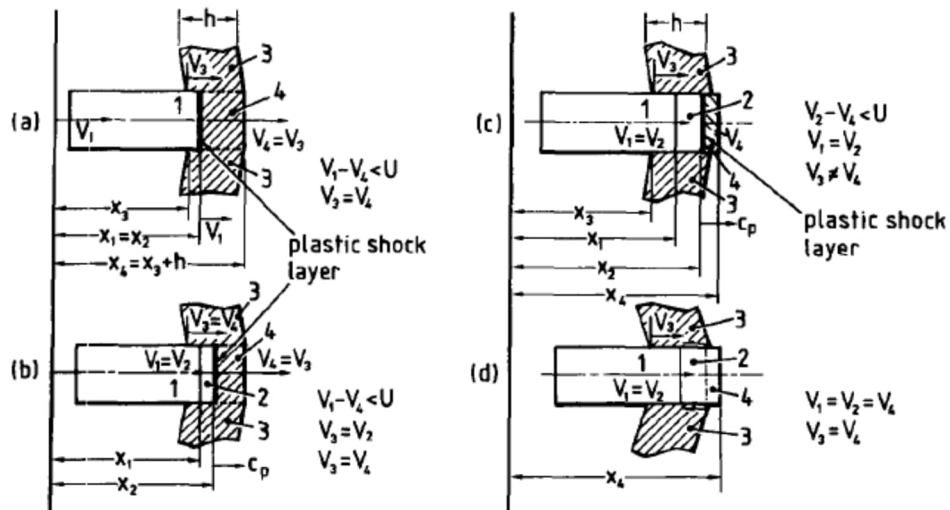
The approach consists in resolving the projectile's movement equation for each step i of the impact process.

$$\frac{d(m_e V_i)}{dt} = -(F_i)$$

For every step, knowing the various F_i forces of resistance involved makes it possible to determine the expression of the projectile's V_i speed of penetration based on the duration and, consequently, deduce the final thickness of penetration or conclude that there will be perforation.

Liss (1983) [Corbett and Reid 1996] suggested a multi-step analytical model that can be used to describe the local effect of an impact by a rigid projectile on a steel target. The process, based on the plastic-wave propagation theory, is broken down into five steps:

- a) penetration phase (indentation);
- b) forming of a cracking cone;
- c) fracture by shearing and uncoupling of the cone;
- d) displacement of the cone;
- e) post-perforation deformation.



1. rigid projectile, 2. deformed part of the cone, 3. proximity of the impact area distorted by plastic rotation, 4. non-deformed part of the cone.

Figure 41: Process of penetration of the projectile in the target on impact [Corbett and Reid 1996]

[Yankelevsky 1997] suggested a two-step analytical model to describe the low-velocity impact on a concrete target.

- Step 1: dynamic penetration phase where the projectile penetrates a semi-infinite medium. Spalling on the rear side is however not taken into account.
- Step 2: plug formation and shear. Upon impact, a plastic wave forms in front of the projectile and travels across the target leading to the progressive formation of a cracking cone through shearing. The cone is then pushed by the projectile, which continues its progression until it has passed completely through the target.

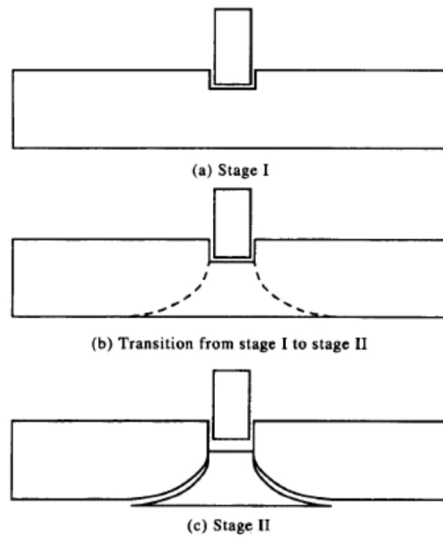


Figure 42: Two-step penetration model [Yankelevsky 1997]

3.3 Numerical methods

Studying the vulnerability of a structure or part of a structure subjected to an impact requires taking into account complex physical phenomena that empirical or analytical models, although widely used, cannot take into account.

The performance of simulation tools and the development of the constituent laws that can be used to represent material behaviour are such that numerical simulation methods are slowly becoming more and more suitable for analysing impact phenomena. In addition to more accurate results, there is the added advantage of the economic benefits compared to full-scale trials.

Amongst the numerical methods, the “continuous” and “discrete” methods can be underlined.

3.3.1 The “continuous” methods

The most widespread continuous methods are methods based on the Finite Elements Method (FEM) with a behaviour law suited to the physics of the problem. The physical systems to study (structures) are discretised in 2 or 3 dimensions using a Finite Element mesh of different types (volumes, shells, beams, bars).

However, impacts lead to the formation and evolution of numerous discontinuities, such as multi-cracking or the propagation of cracks that cannot be reasonably modelled by classic Finite Element Methods.

In order to take into account and address the issue of discontinuities, additional continuous approaches have been developed. The first category consists of adapting the traditional Finite Elements Method and is therefore mesh-based.

The following can be mentioned:

- hydrodynamic approaches with a Eulerian representation that are only really suited for very high-velocity impacts: in this case the matter is uncoupled from the mesh;
- approaches based on the principle of erosion. It consists of removing a finite element from the model when a criterion is met; generally speaking, the criterion used is a plastic deformation threshold;
- approaches based on the introduction of a discontinuity on the interface joining two finite elements. These methods are highly dependent on the mesh;
- approaches based on the introduction of a discontinuity directly into the mesh. Examples are SDA (Strong Discontinuity Approach) or the X-FEM.

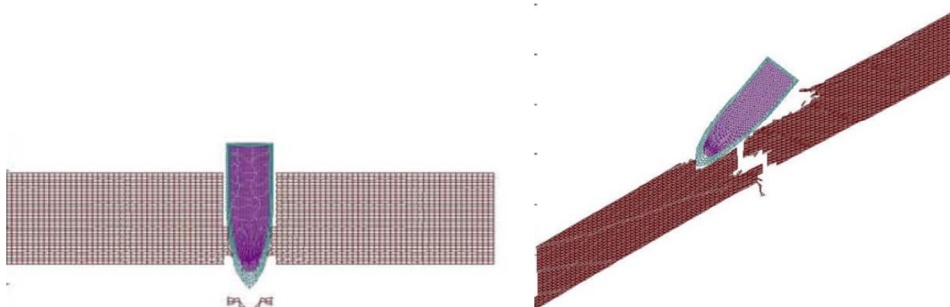


Figure 43: Illustration of the impact of a projectile on a concrete slab [Teng 2004]

Another modelling category regroups the continuous methods qualified as “without mesh”. In this type of representation, nodes are not related to the structure. They offer a better representation of the appearance of discontinuities while keeping the same behaviour laws and do not require adaptive mesh techniques. [Fries et Matthies 2004] suggests a classification of these methods, the most known ones being:

- SPH (Smooth Particles Hydrodynamics): this method is derived from the Lagrangian-context fluid mechanics;
- EFG (Element-Free Galerkin): Methods developed to stabilise the SPH methods.

3.3.2 The “discrete” methods

The “discontinued” or “discrete” methods. They consist of assembling distinct elements – deformable or not – related to one another by very simple laws that represent the material’s behaviour. Unlike the continuous methods, behaviour is not imposed by a constituent law but is a result of the interaction of various elements with one another. The discrete methods are not based on the mechanics of continuous media but are directly resolved by applying the fundamental principle of dynamics to all elements and at each time-step.

These methods are an alternative for analysing the topic of impacts. They bring adequate tools in order to simulate damage, fracturing, propagation of cracks or fragmentation in a more realistic manner. They make it possible to take into account the substantial non-linearities and discontinuities involved.

Different discrete methods exist and can be used, including the Discrete Element Method (DEM). The distinct elements are non-deformable and interact through laws of contact or cohesion. The contact condition is expressed in a “flexible” manner with an equivalent stiffness, and the elements can interpenetrate. They also make it possible to quantitatively reproduce not only the force of impact and the penetration process, but also the transformation of the kinetic energy upon impact.

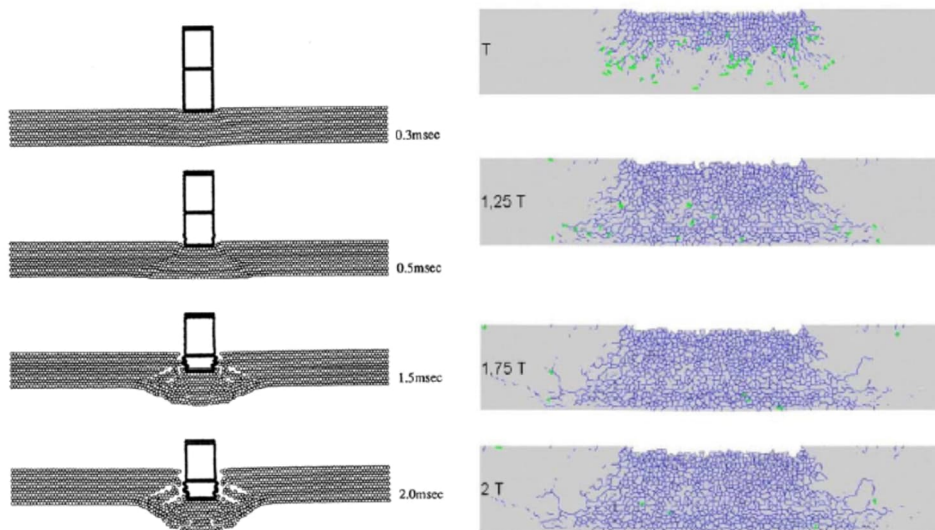


Figure 44: Simulation of the impact of a deformable projectile on a concrete slab using the Discrete Element Method ([Sawamoto et al. 1998] on the left, [Koechlin 2007] on the right)

However, the cost of calculation (model size and duration of the simulation) for these methods can be substantially higher than for the Finite Element Method. Despite being highly effective on small-scale models, they are not suitable when modelling an entire structure and make it very difficult to study the entire structure.

3.3.3 An alternative: the multi-domain approach

Using a multi-domain approach based on the use of combined continuous/discrete methods, such as the FEM/DEM, can be an efficient alternative for simulating the behaviour of structures subjected to impacts, both on a local and an overall scale. The areas close to the impact are modelled by Discrete Elements, since they are likely to present significant discontinuities, whereas the rest of the studied structure or element, subject to less stress, is represented by finite element modelling. A transition area in which both domains are covered can also be defined.

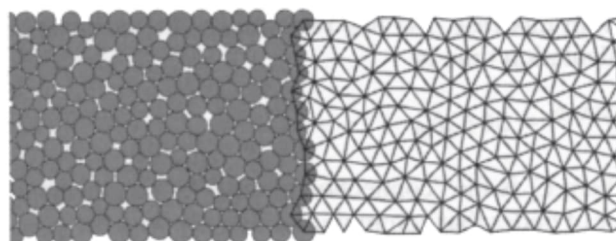


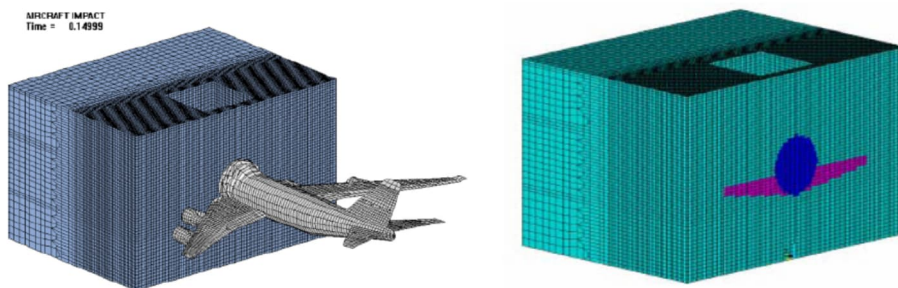
Figure 45: Combined method of finite elements and discrete elements suggested by Cundall (2003) [Frangin 2008]

A reinforced concrete slab can, for example, be modelled using a finite element mesh for the reinforcements and discrete elements for the concrete. This type of approach makes it possible to obtain accurate results while reducing the cost of calculation.



Figure 46: Simulation of the impact of a projectile on a reinforced concrete slab [Frangin 2008]

The choices of model (numerical method, model of the chosen material, etc.) must be suited to the physical phenomenon to be simulated. They must make it possible to represent the main phenomena observed on an experimental basis. For example, the perforation processes following an impact are different depending on if the target is made of concrete or steel. The phenomena involved are also different depending on the nature of the impact (soft impact, hard impact). If the impact is of a hard nature, the duration of the penetration process is generally shorter than the target's overall structure response time. In that case, a purely local analysis seems perfectly relevant. In the event of soft impacts, the duration of impact is a lot longer. Structural waves are generated and travel through the structure. It is generally recommended to study the local behaviour – the local destruction process during perforation – but also the consequences that the propagation of waves may have across the entire structure, i.e. the global behaviour.



(Arros et al., 2006)

Figure 47: Coupled approaches – Impact of a deformable body on a rigid structure [Riera 1968]

3.3.4 Main calculation software programs

It is often difficult to choose a software program for these types of calculations. The main rapid dynamic software programs are Autodyn, LS-DYNA, and Abaqus Explicit. These commercially available software programs are specialised in the responses of structures to impacts. Developed mainly for military applications, their scope of validation is generally limited to supersonic impact velocities. Studies are under way in order to adapt them to the accidental field. Europlexus, Crash and Safer are further examples.

The approach adopted in this type of analysis can be summarised as follows:

1. assume a projectile (size, material, etc.) and a target structure (size, iron framework, thickness, support conditions, etc.) as well as the initial impact conditions (speed of the projectile, location of impact, etc.);

2. choose a method of representation by finite elements or discrete elements or a FEM/DEM combination for the target and the projectile;
3. choose the behaviour laws for the selected materials (reinforced concrete, steel, etc.) both for the target and the projectile (if FEM) or the contact or cohesion laws governing the interaction between the discrete elements (if DEM);
4. choose the typical link conditions between the different elements constituting the target;
5. calculations (resolve the equation system);
6. analyse the results and compare with the damage criteria.

3.3.5 Conclusions

These methods generally require relatively powerful computers, people specialised in this type of calculation, and costs in terms of time and IT resources that are rarely compatible with the constraints pertaining to risk assessments in a regulatory environment.

Furthermore, despite the progress which has been made, rapid dynamic software programs remain very unstable and mesh-dependent. Very few means exist to check the validity of the calculations. It is therefore important to couple these methods with analytical calculations.

4 Protective measures

In order to reduce the vulnerability of a structure to the effects of a projectile impact – and as a result improve its level of protection – reinforcement measures, such as the construction of a protective enclosure or changes to the structure's mechanical properties, can be implemented.

4.1 Protective enclosure

In the case of industrial equipment, building a protective enclosure might be an option. Its walls may be made of metal, concrete or reinforced concrete.

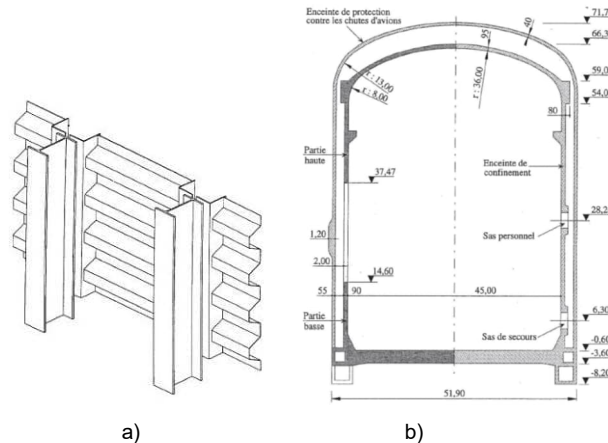


Figure 48: Example of a metal protective wall and a reinforced concrete protective enclosure for a public-access building

For low-impact velocities, installing a splinter-proof protective grating can also be an option. It can be built like the figure below with twisted mesh (as opposed to welded) that deforms when impacted by a projectile. Consequently, the fragment's kinetic energy is dissipated as elongation energy across the steel wires and as friction energy between the meshes.

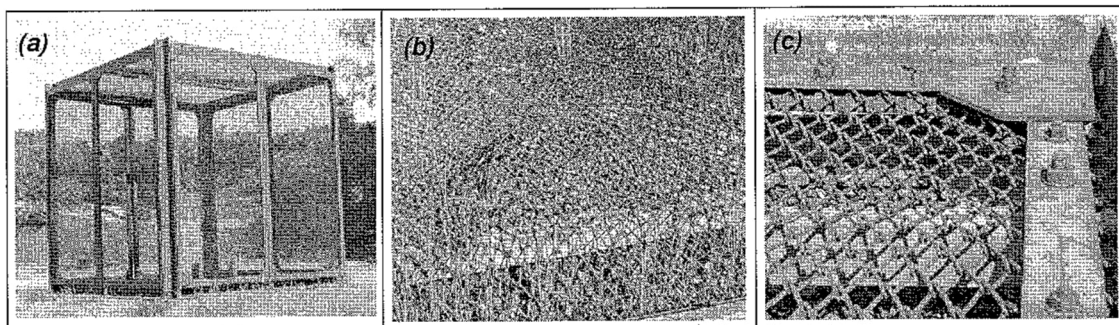


Figure 49: Example of a splinter-proof grating, a) Ineris cage made from splinter-proof grating (4 m x 4 m x 4 m) for burst tests, b) deformation of the grating caused by a projectile, c) attachment to a metal frame

In all cases, the enclosure's different components must be sized, especially in terms of thickness, in order to locally resist the impact – and more importantly perforation – and ensure overall resistance under the effect of the vibrations induced by the shock.

4.2 Changes to the target's mechanical properties

This involves changing the target's mechanical properties by adding matter. The main purpose is to:

- increase the thickness of the target. As a result, the target can absorb a larger quantity of energy without being perforated or destroyed.
- increase the target's resistance capacity, in other words the material's breaking stress. This reduces the projectile's thickness of penetration in the target.

Reinforcements can be masonry units – generally made of concrete or reinforced concrete – or metal components. The thickness of these protective walls can be sized to prevent the projectile from penetrating or so the projectile only partially penetrates the wall of the structure we are trying to protect without causing its general destruction. Remember that the reinforcements must be added in accordance with the equipment's design codes.

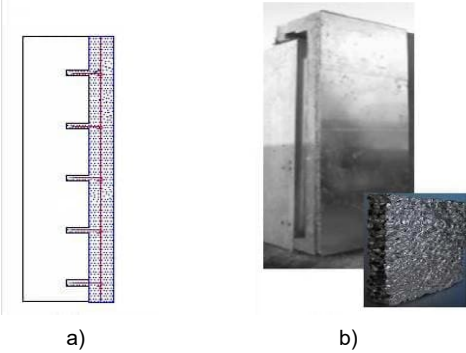


Figure 50: Brickwork and metal reinforcement

5 Conclusion

This document addresses the main issues pertaining to the resistance of structures to impacts.

In reality, this discipline can only be effectively implemented alongside a serious risk assessment. In many cases, this avoids having a too conservative approach or not taking into consideration the proper assumptions on the starting forces.

In order to determine the effects of a projectile impact on concrete or metal structures found on industrial sites, three modelling methods can be considered:

- the empirical approach;
- the analytical approach;
- the numerical approach.

Past experience shows that the analytical approach often leads to economic benefits compared to the empirical approach and does not lead to over-dimensioning of the means of protection being implemented.

The numerical approach must be used with care, and its results must be crossed-checked with an analytical method or experimental trials.

The materials' experimental characterisation, at suitable solicitation intervals that are consistent with the analysis conducted, reduces the uncertainty of the results obtained.

6 Bibliographic references

The most comprehensive bibliographic references for calculating the resistance to impacts are:

[IMFRA 2008] F. MERCIER, Rapport scientifique DRA-08-64041-02123A, Impacts de Fragments BCRD Autorisation de programme 2004 – Convention n°04-00001, 2008.

[Koechlin 2007] P. KOEHLIN, Modèle de comportement membrane-flexion et critère de perforation pour l'analyse de structures minces en béton armé sous choc mou, thèse de Doctorat de l'Université Pierre et Marie Curie – Paris VI, 2007.

[Li 2005] Li, Q.M., Reid, S.R., Wen, H.M., Telford, A.R., 2005. Local impact effects of hard missiles on concrete targets. *Int. J. Impact Eng.* 32 (1–4), 224–284.

[Li 2008] S.Y. Aly, Q.M. Li, 2008, Critical impact energy for the perforation of metallic plates, *Nuclear Engineering and Design* 238, 2521–2528.

[Nguyen 2009] Q.B. NGUYEN, Fiabilité des installations industrielles sous impact de fragments de structures – Effet domino, thèse de Doctorat de l'Université Paris-Est, 2009.

[TM5-1300 1990] TM 5-1300 (NAVFAC P-397, AFR 88-22), "Structures to Resist the Effects of Accidental Explosions," November 1990.

[TNO 2003] Methods for the determination of possible damage to people and objects resulting from the releases of hazardous materials, CPR 16 E, (Green Book), Committee for the prevention of disasters caused by dangerous substances, the Hague: Directorate-General of Labour of the Ministry of Social Affairs and Employment, 1992 – 2003.

[Yankelevsky 1997] Yankelevsky DZ. Local response of concrete slabs to low velocity missile impact. *Int J Impact Eng* 1997; 19(4): 331–43.

The other references used in this section are listed below:

[2010-12] Circular no. 2010-12 of 10 May 2010 summarising the methodological rules applicable to hazard studies, to the assessment of the at-source risk reduction approach and to the technological risk prevention plans (TRPP) in facilities classified under the Law of 30 July 2003.

[2007- 04] Inter-ministerial circular of 20 April 2007 pertaining to the enforcement of the Order of 20 April 2007 setting the rules pertaining to risk assessment and prevention of accidents in pyrotechnic facilities.

[Abbas 1993] Abbas H., Paul D.K., Godbole P.N., Nayak G.C. – Reaction-time response of aircraft crash, *Computers and Structures*, Vol. 55, No. 5, 1995, pp. 809-817.

[Amirikian 1950] Amirikian A. Design of protective structures. Report NT-3726, Bureau of Yards and Docks, Department of the Navy, 1950.

[BNFL 2003] BNFL, 2003. Reinforced concrete slab local damage assessment. R3 Impact Assessment Procedure, Appendix H, vol. 3. Magnox Electric plc & Nuclear Electric Limited.

[CEB 1988], CEB-88, Concrete structures under impact and impulsive loading, 1988.

[Corbett et Reid 1993] Corbett, G.G., Reid, S.R., 1993. Quasi-static and dynamic local loading of monolithic simply-supported steel plates. *Int. J. Impact Eng.* 13, 423–441.

[Corbett and Reid 1996] Corbett, G.G., Reid, S.R., Johnson, W., 1996. Impact loading of plates and shells by free-flying projectiles: a review. *Int. J. Impact Eng.* 18 (2), 141–230.

[Cox and Saville 1985] Cox, B.G and Saville, G. (Eds). High Pressure Safety Code. High Pressure Association, 1975. Reprinted 1985.

[Eibl 1987] Eibl J. – Soft and hard impact, Proc. FIP Congress, The Concrete Society, Concrete for hazard protection, Edinburgh, Scotland, Sept 1987, pp. 175-186.

[Faik 2000] Faik S., Witteman H., 2000, Modeling of impact dynamics: a literature survey, North American ADAMS User Conference 2000.

[Frangin 2008] Frangin E., Adaptation de la méthode des éléments discrets à l'échelle de l'ouvrage en béton armé - Une approche couplée éléments discrets/éléments finis, thèse de doctorat de l'université Joseph Fourier, 2008.

[Fries and Matthies 2004] Fries, T.-P. and Matthies, H.-G. Classification and overview of meshfree methods. Rapport technique, Institute of Scientific Computing, Technical University of Brunswick, Germany, 2004.

- [Forrestal 1994]** Forrestal MJ, Altman BS, Cargile JD, Hanchak SJ. An empirical equation for penetration depth of ogive-nose projectiles into concrete targets. *Int J Impact Eng* 1994; 15(4) :395–405.
- [Fullard 1991]** Fullard K, Baum MR, Barr P. The assessment of impact on nuclear power plant structures in the United Kingdom. *Nucl Eng Des* 1991; 130: 113–20.
- [HSE 1998]** Health and Safety Executive (HSE), Development of methods to assess the significance of domino effect from major hazard sites, 1998.
- [Li and Chen 2003]** Li QM, Chen XW. Dimensionless formulae for penetration depth of concrete target impacted by a nondeformable projectile. *Int J Impact Eng* 2003; 28(1): 93–116.
- [May et al. 2005]** May I.M., Chen Y., Owen D.R.J., Feng Y.T., Bere A.T. – Behaviour of reinforced concrete beams and slabs under drop-weight impact loads, Proc. 6th Asia-Pacific Conference on Shock and Impact Loads on Structures, Perth, Australia, 2005.
- [Mebarki et al. 2007]** 1997. MEBARKI Ahmed, NGUYEN Quoc Bao, MERCIER Frédéric, AMI SAADA Ramdane, REIMERINGER Mathieu. A probabilistic model for the vulnerability of metal plates under the impact of cylindrical projectiles. *Journal of Loss Prevention in the Process Industrial*, 20 (2), 113-186, 2007 (Impact factor in 2006: 0.419).
- [Meder 1982]** Meder G., 1982, Dynamic response of a SDOF elastic-plastic system subjected to aircraft impact pulses, *Nuclear Engineering and Design*, 74, pp 61-74.
- [MICADO 2002]** Méthode pour l'identification et la caractérisation des effets Dominos, mise en place de la directive SEVESO II, 2002.
- [Reid and Wen 2001]** Reid SR, Wen HM, 2001, Predicting penetration, cone cracking, scabbing and perforation of reinforced concrete targets struck by flat-faced projectiles. UMIST Report ME/AM/02.01/TE/G/018507/Z, 2001.
- [Riera 1968]** Riera J.D. – On the stress analysis of structures subjected to aircraft impact forces, *Nuclear Engineering and Design*, Vol. 8, 1968, pp. 415-426.
- [Sawamoto 1998]** Sawamoto, Y., Tsubota, H., Kasai, Y., Koshihara, N. and Morikawa, H. Analytical studies on local damage to reinforced concrete structures under impact loading by discrete element method. *Nuclear Engineering and Design*, 179: 157–177, 1998.
- [Sliter 1980]** Sliter GE, 1980, Assessment of empirical concrete impact formulas. *ASCE J Struct Div* 1980; 106(ST5): 1023–45.
- [SNPE INGENIERIE 1995]** Effets mécaniques de propulsion dans les sphères de gaz liquéfiés, Ref 931934.0/PCL/PCL rev.I - 07 April 1995 (page 11/56).
- [Sugano 1993]** Sugano T., Tsubota H., Kasai Y., Koshika N., Orui S., von Risemann W.A., Bickel D.C., Parks M.B. – Full-scale aircraft impact test for evaluation of impact force, *Nuclear Engineering and Design*, Vol. 140, 1993, pp. 373-385.
- [Teng 2004]** Teng T.L., Chu Y.A., Chang F.A., Chin H.S. Simulation model of impact on reinforced concrete. *Cement and Concrete Research*. 34: 2067-2077, 2004.
- [Thor 1961]** The resistance of various metallic materials to perforation by steel fragments; empirical relationships for fragment residual velocity and weight, Technical Report Project THOR TR No.47, 1961 and No.51, 1963, Ballistic Research Laboratory, Aberdeen Proving Ground, Washington state, USA.
- [USAEC 1974]** Linderman R.B., Rotz J.V., Yeh G.C.K., 1974, Design of structures for missile impact, US Atomic Energy Commission, Topical report.
- [Young 1997]** C.W. Young, 1997, Penetration Equations, Contractor report SAND97-2426.

The more relevant reference guides published by Ineris used alongside this are listed below:

- [Mouilleau 1999]** Guide des méthodes d'évaluation des effets d'une explosion de gaz à air libre (1999) - Ineris - available at www.ineris.fr
- [Heudier 2004]** Omega 15 - Les éclatements de réservoirs / Phénoménologie et modélisation des effets (2004) - Ineris - available at www.ineris.fr
- [Reimeringer 2007]** Formalisation du savoir et des outils dans le domaine des risques majeurs (DRA-35) La résistance des structures aux actions accidentelles (2007) Ineris - available at www.ineris.fr
- [Vallée 2002]** Méthode pour l'identification et la Caractérisation des effets Dominos (MICADO) (2002) – Ineris - available at www.ineris.fr

